Adhesive Contact of an Inflated Circular Membrane with Curved Surfaces

Xingwei Yang[a,*], Abhishek Srivastava[b], Rong Long[a,*]

[a] Department of Mechanical Engineering, University of Colorado Boulder, Boulder, CO 80309, USA.

[b] Corporate Research Laboratory, 3M Company, St. Paul, MN 55144, USA.

* Corresponding authors: xingwei.yang@colorado.edu, rong.long@colorado.edu

Abstract

Inflated elastomeric membranes have been utilized as compliant probes to achieve sensitive adhesion measurement or pneumatic control of adhesive forces. This paper presents an analytical model for the adhesive contact between a circular elastic membrane under inflation and a rigid curved substrate. By adopting an incompressible neo-Hookean model for the membrane and introducing an approximation under large stretch, we obtain analytical solutions describing the three stages of adhesive contact: making contact, contact pinning and delamination. Among these three stages, the making contact stage is assumed to be adhesionless and frictionless, while the other two stages are subjected to a given work of adhesion between the membrane and the substrate. Two limiting cases of tangential interface behaviors (i.e., no slip and frictionless) are considered for the stages of contact pinning and delamination. Our analytical model provides solutions to the deformed membrane profile as well as relationships between key parameters such as applied pressure, contact force, contact radius and displacement, and is verified against computational results from finite element analysis. This analytical model can enable faster solutions for the adhesive contact mechanics of inflated membranes and is applicable as a design, optimization, and system refinement tool for applications such as adhesion measurement, transfer printing and soft robotic gripping.

Keywords

Inflated membrane, large stretch, contact mechanics, adhesion, neo-Hookean model, analytical solution.

1. Introduction

The nonlinear mechanics of soft elastic membranes under inflation has received extensive interests due to its relevance in various engineering applications. Inflation of a circular flat membrane (Hart-Smith and Crisp, 1967) was first studied as an experimental configuration for testing the mechanical behavior of rubber sheets under biaxial tension (Treloar, 1944; Rivlin and Saunders, 1951). Contact between a spherical balloon with internal pressure and two rigid parallel plates (Feng and Yang, 1973) is relevant to the mechanical deformation of biological cells (Hiramoto, 1963; Wan and Liu, 2001). Adhesion needs to be considered in the contact mechanics of inflated membranes when there are attractive interactions on the interface. Indeed, inflated membranes have been used as probes for experimental characterization of adhesion (Shanahan, 1997; Flory et al., 2007; Xu and Liechti, 2011; Laprade et al., 2013). For example, Guvendiren et al. (2009) used an inflated elastomeric membrane to measure the adhesion between a type of molecule found in mussel secreted proteins to different substrates by functionalizing the membrane surface with the adhesive molecule. In comparison to the widely applied Johnson-Kendall-Roberts (JKR) test (Johnson et al., 1971) where solid hemispheres were used as adhesive probes (Chaudhury and Whitesides, 1991; Shull, 2002), inflated membranes can lead to enhanced sensitivity to adhesion by increasing the mechanical compliance of contact (Flory et al., 2007). Another useful feature of using inflated membranes as probes is that their adhesive force with another surface can be tuned by the applied pressure (Dening et al., 2014; Plaut, 2022a, 2022b), thereby opening the door to pneumatic control of adhesive force for applications such as transfer printing (Carlson et al., 2012) and soft robotic gripping (Song and Sitti, 2014; Song et al., 2017). More recently, it has been demonstrated that by inflating or deflating a suspended elastic membrane on a device, one can achieve switchable adhesive strength through the suction cup effect (Song et al., 2021; Frey et al., 2022) or rigidity tuning (Swift et al., 2020).

From a theoretical perspective, the adhesive contact mechanics of pressurized elastic films have been studied and reported in numerous previous works. Among these works, the underlying elastic film was modeled as a plate with purely bending deformation (Plaut et al., 2003), a membrane with purely stretching deformation (Williams, 1997; Plaut et al., 2003; Xu and Liechti, 2011; Zhu et al., 2017, 2018), or a von Karman plate with both bending and stretching deformation (Plaut et al., 2003). It has been shown that if the film is thin and subjected to large deflection or pre-stretch, the membrane model with purely stretching deformation is more appropriate

(Komaragiri et al., 2005; Long et al., 2010), which is the regime considered in this work. Specifically, here we analyze the problem of an inflated circular membrane in adhesive contact with a rigid substrate, as schematically illustrated in Fig.1. To enhance the generality of our model, we assume the substrate surface to be spherically curved with a radius of curvature R_s (see Fig.1). The special case of flat substrate is recovered by taking the limit of R_s approaching infinity. This problem is motivated by the applications of membrane-based adhesion test (Laprade et al., 2013) or soft robotic gripper (Song and Sitti, 2014). In these applications, the membrane often undergoes large deflection which can also lead to large stretch within the membrane. To capture the nonlinear effects associated with large deflection and stretch, finite deformation kinematics and hyperelastic constitutive relations (Libai and Simmonds, 1998) should be used to model the membrane deformation, which requires one to solve a set of nonlinear differential equations (Long et al., 2010). Moreover, the boundary conditions associated with adhesive contact can change as the contact area evolves. Therefore, solving the nonlinear membrane deformation upon adhesive contact can be a challenging task. Existing studies in the literature mostly rely on numerical methods (Long et al., 2010; Sohail et al., 2013; Srivastava and Hui, 2013; Patil et al., 2014, 2015). In comparison to numerical methods, analytical methods can enable faster solutions and thus are advantageous for exploring the parametric space during design or controlling the adhesive force (e.g., for soft robotic gripper).

This work aims to develop an analytical model for the membrane contact problem illustrated in Fig.1. It should be mentioned that Song et al. (2019) recently developed an analytical model for the adhesion of inflated circular membranes on curved surfaces. Their model approximated the deformed shape of free standing membrane (i.e., the membrane outside the contact region) as a truncated cone, and was shown to capture the experimentally observed detachment process. However, they also noted discrepancy due to the truncated cone approximation and suggested a more accurate analysis to be carried out. Recently we presented a set of analytical solutions for the Hertzian contact (i.e., frictionless and adhesionless) between an inflated membrane with various surfaces (Yang et al., 2021). These solutions were based on an approximation found by Foster (1967a, 1967b) for membranes made of the incompressible neo-Hookean solid under large stretch. Here we extend this approach to adhesive contact. Specifically, Section 2 briefly summarizes the analytical solution of inflated neo-Hookean membrane with large stretch and discusses the boundary conditions for adhesive contact. The solutions for adhesive contact are presented in

Section 3. Note that our solutions do not rely on any assumption regarding the deformed shape of the membrane. To demonstrate the accuracy of our solutions, we build a Finite Element Analysis (FEA) model to simulate the adhesive contact process of an inflated neo-Hookean membrane, and compare our analytical solutions to the FEA results. The model for FEA simulation is described in Section 4. In Section 5, we illustrate our solutions and the comparisons with FEM results for two different contact scenarios inspired by soft robotic gripping (e.g., Fig.1c) and membrane based adhesion tests (e.g., Fig.1d). Conclusions are given in Section 6.

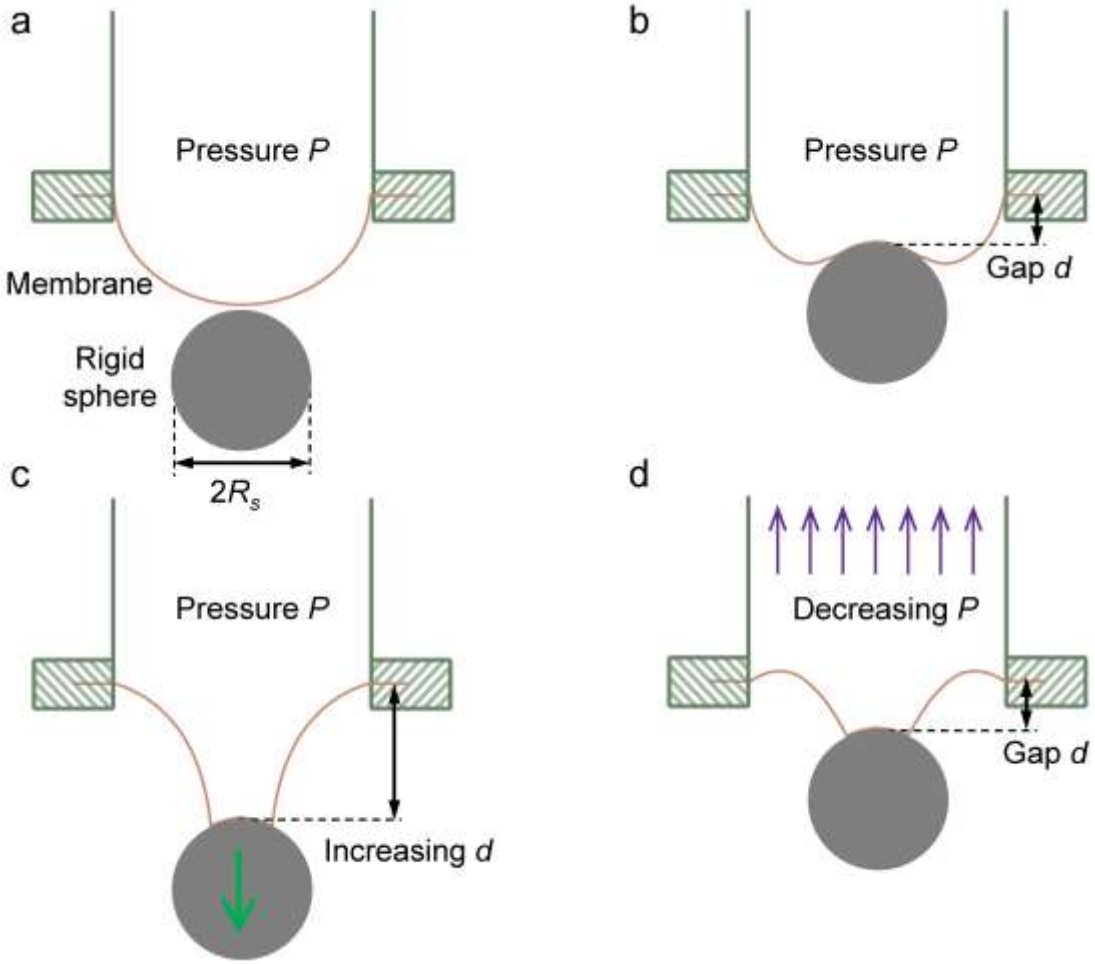

Figure 1. Schematics of adhesive contact between an inflated circular membrane and a rigid spherical surface. (a) The inflated membrane is placed above the rigid sphere with radius R_s with their axes of symmetry aligned. (b) Contact between the inflated membrane and the rigid sphere can be established by either increasing the pressure P or decreasing the gap d. (c) Membrane delamination by increasing the gap d under a fixed pressure P. (d) Membrane delamination by decreasing the pressure P under a fixed gap d.

2. Analytical Model

2.1 Axisymmetric membrane deformation: kinematics and equilibrium

To analyze the adhesive contact problem illustrated in Fig.1, we first define the membrane geometry and describe the underlying assumptions. As shown in Fig.2a, the membrane in its undeformed configuration has a flat circular shape with radius β and thickness h. Before inflation, the membrane is subjected to a uniform equibiaxial pre-stretch λ_0 and then is fixed at its edge. The pre-stretched membrane, with a radius of $b = \lambda_0\beta$, deforms under a uniform pressure P and makes contact with a rigid, spherically curved substrate with radius R_s. Both the deformed membrane and the spherical substrate are axisymmetric. We assume that their axes of symmetry are aligned so that their contact area has a circular boundary. The size of contact area can be controlled by varying the pressure P or the gap d between the membrane's edge and the substrate (Fig.1b). For example, in the experiments of Laprade et al. (2013), the membrane was placed at a fixed gap d above the substrate and was inflated under an increasing pressure P. Contact was established when P is sufficiently large, while delamination was achieved by decreasing P (Fig.1d). Alternatively, one can use the inflated membrane as an adhesive probe, i.e., indenting the inflated membrane on the substrate by lowering the gap d and then detaching the membrane from the substrate by increasing d (Fig.1c). In this case, the inflated membrane resembles the elastic hemisphere used in a JKR test (Shull, 2002).

It has been widely observed that the adhesion between two surfaces is smaller when they are approaching each other (i.e., making contact) than when they are being separated from an established contact interface (Chaudhury and Whitesides, 1991; Vajpayee et al., 2008). Motivated by this phenomenon known as "adhesion hysteresis" (Shull, 2002), we assume Hertzian contact (i.e., frictionless and adhesionless) between the membrane and the substrate when they are making contact, and adhesive contact when the membrane is being detached from the substrate. The former problem of Hertzian contact has been solved in our recent work (Yang et al., 2021). This work focuses on the latter problem of adhesive contact. Our goal is to obtain analytical solutions that can relate the pressure P, the gap d, the radius of contact area a, and the contact force F which is the total force exerted on the membrane by the substrate and is positive in compression.

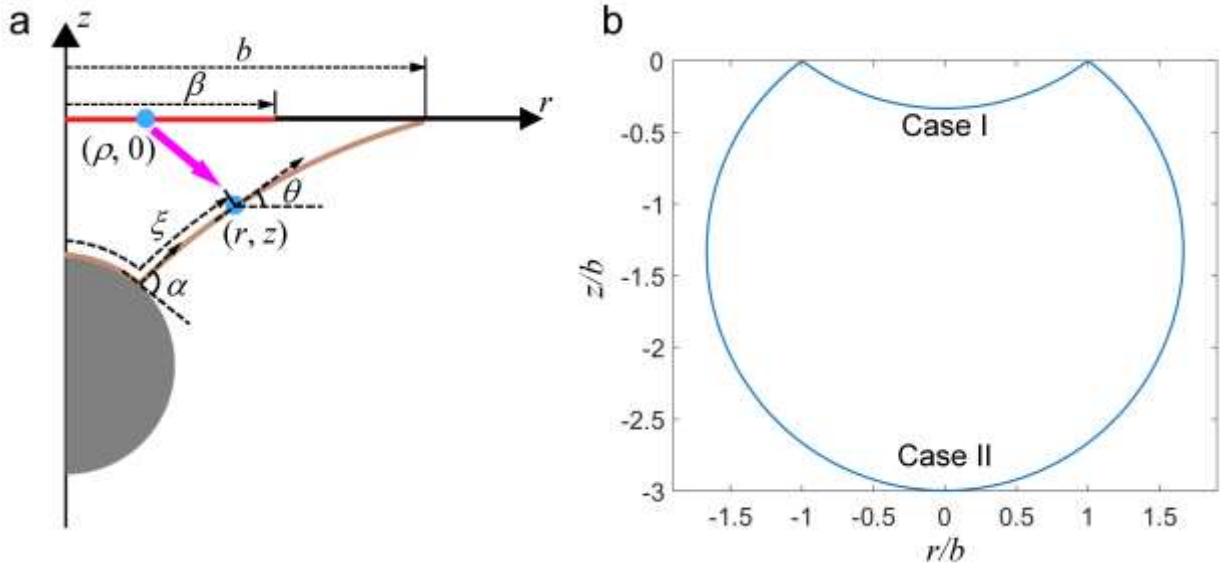

Figure 2. Axisymmetric membrane deformation. (a) A schematic showing the kinematics of membrane deformation. The material point at $(\rho, 0)$ in the undeformed membrane (i.e., the red line) is displaced to (r, z) in the deformed membrane (i.e., the brown curve). Here the deformed membrane is illustrated using the case in Fig.1c as an example, i.e., the membrane is undergoing delamination while subjected to a pressure P. The contact angle α is defined as the angle between the free standing membrane and the tangential direction of the spherical substrate at the contact edge. (b) The two cases of solutions for an incompressible neo-Hookean membrane under free inflation with $Pb/2\mu h = 0.6$ (or $R/b = 1.67$).

Our analysis is based on the well-established hyperelastic membrane theory (Libai and Simmonds, 1998). Recall that the membrane only undergoes stretching deformation, i.e., it is so thin that its bending rigidity is negligible. Specifically, each material point in the membrane is subjected to two principal stretch ratios within the tangential plane of the membrane surface (i.e., the in-plane stretch ratios) and a principal stretch ratio along the thickness direction of the membrane. Also, the stretching deformation is assumed to be uniform across the membrane thickness. This implies that the stretch ratios in the membrane only depend on the two in-plane coordinates of the undeformed membrane. Further simplification is enabled by the axisymmetry of our problem, i.e., the membrane surface can be described by a curve in the r-z plane of a cylindrical coordinate system (r, ϕ, z). The origin of this coordinate system is located at the center

of the undeformed membrane which is represented by a line segment from $r = 0$ to $r = \beta$ (Fig.2a). Therefore, the stretch ratios in the membrane are only a function of the coordinate ρ ($0 \leq \rho \leq \beta$) along the undeformed membrane. After deformation, a generic point $(\rho, 0)$ in the undeformed membrane is displaced to (r, z), forming a curve for the deformed membrane (Fig.2a). Because of axisymmetry, the two in-plane principal stretch ratios, denoted as λ_1 and λ_2, are along the longitudinal direction (i.e., within the r-z plane) of the deformed membrane and the latitudinal direction (i.e., along the ϕ-direction). In particular, λ_1 quantifies the stretch from a segment $d\rho$ in the undeformed membrane to $d\xi$ in the deformed membrane in the r-z plane (ξ is the arc length along the deformed membrane; see Fig. 2a), while λ_2 quantifies the stretch from a circular perimeter of $2\pi\rho$ along the ϕ-direction of the undeformed membrane to $2\pi r$ in the deformed membrane:

$$\lambda_1 = \frac{d\xi}{d\rho}, \tag{1}$$

$$\lambda_2 = \frac{r}{\rho}. \tag{2}$$

The principal stretch ratios λ_1 and λ_2 correspond to two principal tensile stresses within the tangential plane of the deformed membrane. Since the principal tensile stresses are uniform across the thickness direction, one can multiply them by the membrane thickness and define the principal line tensions (force per unit length). The principal line tensions along the directions of λ_1 and λ_2 are denoted as T_1 and T_2, respectively. Equilibrium along the normal direction and the longitudinal direction (i.e., along the arc length ξ) of the deformed membrane requires (Long and Hui, 2012; Yang et al., 2021):

$$T_1 \frac{d\theta}{d\xi} + T_2 \frac{\sin\theta}{r} = P, \tag{3}$$

$$\frac{d\left(T_1 r\right)}{dr} = T_2, \tag{4}$$

where θ is the angle between the longitudinal tangent of the deformed membrane and the r-axis (see Fig.2a) and is given by

$$\cos\theta = \frac{dr}{d\xi},\ \sin\theta = \frac{dz}{d\xi}. \tag{5}$$

If the applied pressure P is uniform, one can substitute eq. (4) into eq. (3) and integrate with respect to r, which gives (Long and Hui, 2012; Yang et al., 2021):

$$\sin\theta = \frac{P\left(r^2 + C_1\right)}{2T_1 r} \tag{6}$$

where C_1 is an integration constant.

2.2 Approximation for neo-Hookean membrane under large stretch

The line tensions T_1 and T_2 are governed by the stretch ratios λ_1 and λ_2 through the hyperelastic constitutive relation of the membrane. Here we adopt the incompressible neo-Hookean model with the following strain energy density function:

$$W = \frac{\mu}{2}\left(\lambda_1^2 + \lambda_2^2 + \lambda_3^2 - 3\right), \tag{7}$$

where μ is the shear modulus of the membrane and λ_3 is the out-of-plane principal stretch ratio. Incompressibility implies that λ_3 is related to the two in-plane principal stretch ratios λ_1 and λ_2 by $\lambda_3 = 1/(\lambda_1\lambda_2)$. Using eq. (7), we first evaluate the two in-plane principal Cauchy stresses and multiply them by the deformed membrane thickness $\lambda_3 h$ to obtain the line tensions T_1 and T_2 (Long and Hui, 2012):

$$T_1 = \mu h\left(\frac{\lambda_1}{\lambda_2} - \frac{1}{\lambda_1^3\lambda_2^3}\right), \tag{8}$$

$$T_2 = \mu h\left(\frac{\lambda_2}{\lambda_1} - \frac{1}{\lambda_1^3\lambda_2^3}\right). \tag{9}$$

It should be noted that eqs. (8) and (9) rely on the plane stress approximation that the out-of-plane principal stress is zero. Although a pressure P is applied on the membrane surface, it is much smaller than the in-plane tensile stresses and thus can be neglected in the constitutive relation of T_1 and T_2 (Libai and Simmonds, 1998).

Under very large stretch ($\lambda_1 >> 1$ and $\lambda_2 >> 1$), the term $\lambda_1^{-3}\lambda_2^{-3}$ in eqs. (8) and (9) is negligible in comparison to λ_1/λ_2 or λ_2/λ_1, leading to the following approximation,

$$T_1 \approx \mu h \frac{\lambda_1}{\lambda_2} \approx \mu^2 h^2 \frac{1}{T_2}. \tag{10}$$

Foster (1967a) discovered that by using eqs. (6) and (10), one can further integrate eq. (3) to obtain the following expression:

$$\sin^2\theta = \frac{P^2\left(r^2 + C_1\right)^2}{4\left(\mu^2 h^2 r^2 + C_2\right)} \tag{11}$$

where C_1 is the constant in eq. (6) and C_2 is an additional integration constant. A detailed derivation of eq. (11) can be found in our recent work (Yang et al., 2021). Once C_1 and C_2 are determined using boundary conditions, eq. (11) governs how the angle θ varies along the deformed membrane (i.e., as r varies), from which one can obtain the profile of the deformed membrane by integrating $dz/dr = \tan\theta$.

2.3 Free inflation

Before the membrane can make contact with the substrate, its deformation is solely due to the applied pressure P. This case is referred to as free inflation and has been solved in our previous work (Yang et al., 2021). Here we briefly review this case to demonstrate the determination of C_1 and C_2 from boundary conditions. Under free inflation, the center of the deformed membrane is flat and subjected to equi-biaxial stretch:

$$\theta = 0,\ \lambda_1 = \lambda_2 \text{ at } r = 0 \tag{12}$$

The former condition ($\theta = 0$ at $r = 0$) and eq. (6) imply that $C_1 = 0$. The latter condition ($\lambda_1 = \lambda_2$ at $r = 0$) and eq. (10) imply that

$$T_1 = T_2 \approx \mu h \text{ at } r = 0 \tag{13}$$

By substituting eq. (13) into eq. (6) and comparing the resulting equation with eq. (11), we conclude that $C_2 = 0$. Therefore, eq. (11) becomes

$$\sin^2\theta = \left(\frac{P}{2\mu h} r\right)^2 . \tag{14}$$

Based on eq. (14), one can use $(dz/dr)^2 = \tan^2\theta = \sin^2\theta/(1-\sin^2\theta)$ to obtain the deformed membrane profile $z(r)$ by integrating dz/dr and enforcing the boundary condition at the fixed edge (i.e., $z = 0$ at $r = b$). As detailed in Yang et al. (2021), the resulting membrane profile is a spherical cap with radius $R \equiv 2\mu h/P$. However, there are two possible solutions under the same pressure P, which are essentially the two caps of one sphere with radius R and are referred to as Case I and II (see Fig.2b for example). Mathematically these two solutions can be obtained by restricting θ to be smaller than $\pi/2$ at the fixed edge $r = b$ (Case I) or allowing θ to be larger than $\pi/2$ at $r = b$ (Case II). The non-uniqueness of free inflation solutions for the neo-Hookean membrane is well known in the literature (Foster, 1967b; Hassager et al., 1999). In particular, Case II corresponds to an unstable branch of solutions where the membrane deflection decreases with the pressure (Yang et al., 2021). For simplicity, here we focus our study for adhesive contact on the stable branch (i.e., Case I). For Case I solutions, the deflection at the apex of the inflated membrane, denoted as d_0, is given by

$$d_0 = -z(r=0) = \frac{2\mu h}{P} - \sqrt{\left(\frac{2\mu h}{P}\right)^2 - b^2} . \tag{15}$$

Equation (15) is useful for the solutions of membrane contact since it provides the initial value of gap d (see Fig.1b) when the apex of the inflated membrane just reaches the substrate.

2.4 Adhesionless contact

When the gap d is smaller than d_0, the inflated membrane makes contact with the substrate and establishes a circular contact area with a circular boundary whose radius is denoted as a (see Fig.3a). During this making contact stage, the membrane/substrate contact is assumed to be adhesionless and frictionless. This problem has also been solved in our previous work (Yang et al., 2021). Briefly, the membrane within the contact area conforms to the substrate and hence has the shape of a spherical cap with radius R_s. This implies that the contacting membrane is effectively inflated by $P_e - P$, where P_e is the uniform contact pressure from the substrate and P is the applied

pressure. Using the free inflation solution, we can obtain the following equation for the contact pressure P_e:

$$P_e = P + \frac{2\mu h}{R_s}. \tag{16}$$

Note that in the special case of a flat substrate, R_s approaches infinity and hence $P_e = P$. The compressive contact force F is

$$F = \pi a^2 P_e. \tag{17}$$

The contact radius a (see Fig.3a) needs to be solved using the membrane profile outside the contact area. Specifically, we utilize the boundary conditions that the tangent angle θ and the stretch ratios (λ_1 and λ_2) are continuous at the edge of the contact area for adhesionless contact (Yang et al., 2021). First, the tangent angle at the contact edge ($r = a$) is

$$\theta(r = a) = \theta_a = \arcsin(-a / R_s), \tag{18}$$

where θ_a is the angle between the tangential direction of the substrate at the contact edge and the horizontal direction (see Fig.3a). Second, since the membrane within the contact area makes conformal contact with the substrate, it has a spherical profile and is subjected to equi-biaxial stretch. Therefore, at the contact edge ($r = a$) we expect that $\lambda_1 = \lambda_2$. Using these two boundary conditions, one can determine the two constants C_1 and C_2 in eq. (11) as

$$C_1 = \frac{2\mu h a \sin\theta_a}{P} - a^2 = -\left(1 + \frac{R}{R_s}\right)a^2 \text{ and } C_2 = 0. \tag{19}$$

Recall that $R = 2\mu h/P$ is the radius of the freely inflated membrane with pressure P. Using eq. (19), we can rewrite eq. (11) as

$$\sin^2\theta = \frac{\left(r^2 - (1 + R/R_s)a^2\right)^2}{R^2 r^2}. \tag{20}$$

The membrane profile $z(r)$ outside the contact area can be obtained by integrating dz/dr determined from eq. (20) and enforcing the boundary condition at the fixed edge ($z = 0$ at $r = b$) (Yang et al., 2021). This leads to closed-form analytical solutions for the membrane profile as well as relations between the contact radius a, the applied pressure P, the contact force F and the gap d. Here we

will use these analytical solutions to describe the making contact stage between the inflated membrane and the substrate (Fig.1b). If the making contact stage is controlled by reducing the gap d, it is useful to define the contact displacement δ as the difference between d and d_0 (eq. (15)):

$$\delta = d_0 - d \,. \tag{21}$$

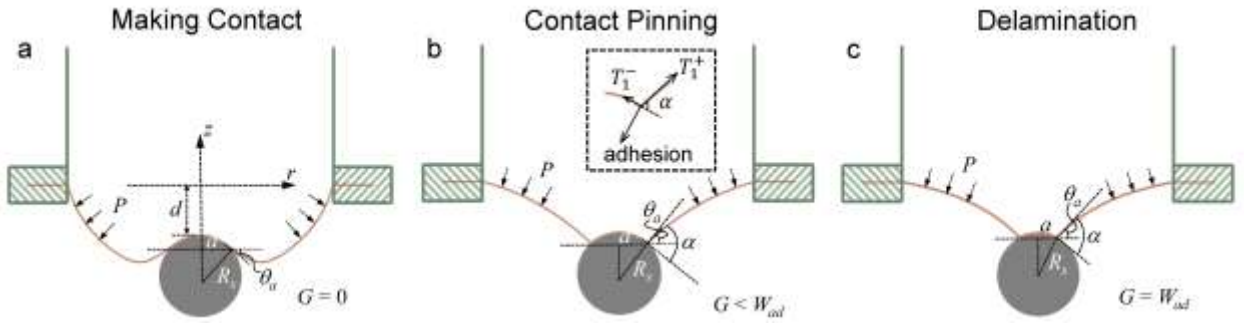

Figure 3. The three stages of contact between the inflated membrane and the spherical substrate. (a) The making contact stage where the membrane makes adhesionless and frictionless contact with the upper hemisphere of the substrate under increasing pressure P or decreasing gap d. (b) The contact pinning stage where the membrane has a tendency of being detached from the substrate due to the reversal of external loading (i.e., decreasing P or increasing d). Here the contact interface between membrane and substrate becomes adhesive which resists the tendency of detachment ($G < W_{ad}$). The inset shows that a contact angle α and a discontinuity in the longitudinal line tension T_1 can develop at the contact edge. (c) The delamination stage where the membrane is continuously detaching from the substrate in a quasi-static manner ($G = W_{ad}$) under decreasing P or increasing d.

2.5 Adhesive contact

After a certain contact radius (denoted as $a = a_m$) is established in the making contact stage, the membrane is retracted from the substrate either by increasing the gap d (Fig.1c) or reducing the pressure P (Fig. 1d). During retraction, the contact between membrane and substrate is adhesive. Adhesion could be captured by introducing attractive tractions between the membrane and substrate surfaces through a cohesive zone model (Hui et al., 2011). However, this would make it difficult to derive analytical solutions. Here we follow the energetic approach adopted in the JKR

theory (Johnson et al., 1971) and represent the effect of adhesion by the energy required to separate a unit area of interface which is defined as the work of adhesion W_{ad}. In this approach, adhesion can provide a concentrated force pinning the contact edge (Fig. 3b), thereby enabling discontinuities at the contact edge in terms of the tangential direction, stretch ratio, and tension of the deformed membrane. For example, the non-contacting membrane does not need to remain tangential to the substrate at the contact edge. Instead, it can make a contact angle of α with the substrate (Fig. 3b), which is related to the tangent angle θ at the contact edge through the following equation:

$$\theta(r=a)=\theta_a=\alpha-\arcsin\left(a/R_s\right)\ . \tag{22}$$

Note that for adhesionless contact, $\alpha = 0$ and eq. (18) is recovered. Also, the longitudinal stretch ratio λ_1 can be discontinuous across the contact edge, while the latitudinal stretch ratio λ_2 must remain continuous due to the continuity in r (see eq. (2)). Because of the discontinuity in λ_1 at the contact edge, we denote its value within and out of the contact region as λ_1^- and λ_1^+, respectively.

Whether the membrane can be detached from the substrate is governed by an energetic criterion that compares the energy release rate G with the work of adhesion W_{ad}. It was derived (Long et al., 2010) that the energy release rate for a neo-Hookean membrane under axisymmetric deformation is

$$G=T_1^+\left(1-\cos\alpha\right)+\frac{\mu h}{2}\left[\frac{\left(\lambda_1^+-\lambda_1^-\right)^2}{\lambda_1^-\lambda_2}+\frac{1}{\left(\lambda_1^-\lambda_2\right)^3}\left(1-3\left(\frac{\lambda_1^-}{\lambda_1^+}\right)^2+2\left(\frac{\lambda_1^-}{\lambda_1^+}\right)^3\right)\right], \tag{23}$$

where T_1^+ is the longitudinal membrane tension right outside the contact edge and can be determined using eq. (8) with the stretch ratios λ_1^+ and λ_2 at the contact edge. At the beginning of the retracting stage, $G < W_{ad}$ so that the contact edge remains pinned by adhesion, which will be referred to as the contact pinning stage. During this stage, only the non-contacting membrane responds to the external loading (e.g., increasing gap d or decreasing pressure P), causing the energy release rate G to increase. Once G becomes equal to W_{ad}, the membrane starts to be detached from the substrate. This is the delamination stage during which the membrane is peeled from the substrate and the equilibrium condition $G = W_{ad}$ is maintained for quasi-static peeling. It

is worth mentioning that for adhesionless contact (Section 2.4), the contact angle α is zero and the stretch ratio λ_1 is continuous across the contact edge (i.e., $\lambda_1^- = \lambda_1^+$). Plugging these two conditions into eq. (23) results in $G = 0$, which is expected for adhesionless contact.

Apart from the adhesion criterion, we also need to specify the tangential behavior of the interface, i.e., whether relative slip is allowed between the membrane and the substrate within the contact region. Early analyses on membrane peeling assume no interfacial slip between the contacting membrane and substrate (Kendall, 1971, 1975; Gent and Kaang, 1986; Williams, 1997; Wan, 1999). More recently, it has been experimentally observed that the contacting membrane can slide on the substrate while maintaining adhesion with it (Newby and Chaudhury, 1997, 1998; Begley et al., 2013). Such slip is induced by the tangential component of the peel force and depends on the adhesive interface. For example, Newby et al. (1995) showed that interfacial slip can be controlled by functionalizing the substrate through a self-assembled monolayer. While the effect of interfacial slip can be modeled by accounting for the mixed-mode condition of interface fracture (Cheng et al., 2012), this would require a detailed characterization of the mode-dependent adhesion as well as a local stress analysis at the interface crack tip (i.e., the contact edge) to determine the mode-mixity (Hutchinson and Suo, 1991). To probe the effect of interfacial slip while keeping the analysis tractable, we consider two limiting cases: no-slip and frictionless (Long et al., 2010), which are also known as "sticking" contact and "sliding" contact, respectively (Wang and Li, 2007; Begley et al., 2013; Collino et al., 2014). The former assumes infinite resistance to interfacial slip while the latter assumes zero resistance. These two cases entail different boundary conditions at the contact edge, which will be discussed in the following section.

3. Solutions of adhesive contact

Here we derive solutions for the membrane contact problem using the governing equations and boundary conditions outlined in Section 2. These solutions are organized according to the three stages illustrated in Fig.3. Recall that during the first stage ("making contact"), the membrane/substrate contact is assumed to be adhesionless and frictionless, while adhesion is included during the next two stages ("contacting pinning" and "delamination") with either no-slip or frictionless condition.

3.1 Making contact

During this stage, the membrane profile outside the contact region ($r \geq a$) can be determined by integrating eq. (20). As systematically discussed in our previous work (Yang et al., 2021), there are several branches of solutions depending on the range of θ. Here we focus on Case I inflation (see Fig.2b and Section 2.3) with $\theta < \pi/2$ at the fixed edge $r = b$. Moreover, we assume the contact area is within the upper hemisphere of the substrate. These two assumptions imply that the range of θ is from $-\pi/2$ to $\pi/2$. Using this range and eq. (20), it can be derived that the non-contacting membrane profile is given by

$$z(r) = -\int_r^b \frac{\left(s^2 - \left(1 + R/R_s\right)a^2\right)}{b\sqrt{R^2 s^2 - \left(s^2 - \left(1 + R/R_s\right)a^2\right)^2}} ds \qquad (a \leq r \leq b)\,, \tag{24}$$

where s is an integration variable, $R = 2\mu h/P$, and R_s is the radius of the spherical substrate. Based on eq. (24), the gap d between the membrane's fixed edge and the apex of the substrate is

$$d = \int_a^b \frac{\left(s^2 - \left(1 + R/R_s\right)a^2\right)}{b\sqrt{R^2 s^2 - \left(s^2 - \left(1 + R/R_s\right)a^2\right)^2}} ds - R_s + \sqrt{R_s^2 - a^2}\,. \tag{25}$$

In addition, the contact force F given in eq. (17) can be rewritten as follows using eq. (16):

$$F = \pi a^2 P\left(1 + R/R_s\right). \tag{26}$$

The membrane profile within the contact region is a spherical cap with radius R_s. Since the contact interface is adhesionless and frictionless, the tractions exerted by the substrate on the membrane are normal to the interface (i.e., the contact pressure P_e) and should be uniformly distributed to maintain the spherical profile of the contacting membrane (Yang et al., 2021). To facilitate the calculation of the energy release rate G during retraction, it is important to determine the stretch ratios in the contacting membrane. We use the fact that the contacting membrane is subjected to equi-biaxial tension, i.e., $\lambda_1 = \lambda_2$, due to its spherical profile (Yang et al., 2021). Note that this does not imply that λ_1 and λ_2 are uniform in the contacting membrane. Instead, λ_1 and λ_2 are larger at the center of the contacting membrane and decrease as the contacting edge is approached (Yang et al., 2021). Using the condition $\lambda_1 = \lambda_2$ and eqs. (1), (2) and (5), we can write the following equation for the contacting membrane ($r < a$):

$$\frac{d\xi}{d\rho} = \frac{1}{\cos\theta}\frac{dr}{d\rho} = \frac{r}{\rho}. \tag{27}$$

The spherical profile of the contacting membrane leads to the following identity:

$$\cos\theta = \sqrt{1-\frac{r^2}{R_s^2}} \quad \text{for } r < a. \tag{28}$$

Substituting eq. (28) into eq. (27) and integrating from the center of the contacting membrane (r = 0 and ρ = 0), we have

$$\int_0^{r^*} \sqrt{\frac{R_s^2}{R_s^2 - r^2}}\frac{1}{r}dr = \int_0^{\rho^*}\frac{1}{\rho}d\rho, \tag{29}$$

where r^* (< a) represents a generic point within the contacting membrane and ρ^* is the corresponding material coordinate. There is a removable singularity in eq. (29) at the center (r = 0 and ρ = 0). To address this issue, we denote the equi-biaxial stretch ratio at the center as λ_c and replace the lower integral limits in eq. (29) by $r = \varepsilon$ and $\rho = \varepsilon/\lambda_c$ where ε is a small length ($\varepsilon << a$). This allows us to integrate eq. (29) and obtain

$$\ln\left(\frac{1+\sqrt{1-\left(\varepsilon/R_s\right)^2}}{1+\sqrt{1-\left(r^*/R_s\right)^2}}r^*\right) - \ln\varepsilon = \ln\left(\lambda_c\rho^*\right) - \ln\varepsilon. \tag{30}$$

The removable singularity of eq. (29) is reflected in the $\ln\varepsilon$ term as ε approaches 0. Cancelling the $\ln\varepsilon$ term on both sides and taking the limit of $\varepsilon \to 0$, we have

$$\lambda_1\left(r^*\right) = \lambda_2\left(r^*\right) \equiv \frac{r^*}{\rho^*} = \lambda_c\frac{1+\sqrt{1-\left(r^*/R_s\right)^2}}{2} \quad \text{for } r^* < a. \tag{31}$$

Equation (31) can also be recast into the function $\rho^*(r^*)$, i.e., the material coordinate at any point ($r^* < a$) within the contact region. It is worth noting that if the substrate is flat, R_s approaches infinity and hence eq. (31) is reduced to $\lambda_1(r^*) = \lambda_2(r^*) = r^*/\rho^* = \lambda_c$, implying that the contacting membrane is under uniform equi-biaxial stretch. This is expected given that the contact interface is flat and frictionless.

Although eq. (31) specifies the variation of stretch ratios within the contacting membrane, it is subjected to an unknown coefficient λ_c. This coefficient can be determined by considering the non-contacting membrane ($r \geq a$). Specifically, combining eqs. (6) and (11), we find that the non-contacting membrane must satisfy

$$T_1^2 = \mu^2 h^2 + \frac{C_2}{r^2} \qquad (r \geq a). \tag{32}$$

Moreover, after applying the approximation in eq. (10) and using eqs. (1), (2) and (5), we obtain

$$\frac{1}{\cos^2\theta}\left(\frac{dr}{d\rho}\right)^2 = \frac{\mu^2 h^2 r^2 + C_2}{\mu^2 h^2 \rho^2} \quad (r \geq a). \tag{33}$$

Given that the non-contacting membrane satisfies eq.(20) and $C_2 = 0$ according to eq. (19), we can rewrite eq. (33) as

$$\frac{1}{\sqrt{r^2 - \left(r^2 - \left(1 + R/R_s\right)a^2\right)^2 / R^2}}\, dr = \frac{1}{\rho}\, d\rho \ \text{ for } r \geq a, \tag{34}$$

where we have applied the condition that θ is between $-\pi/2$ to $\pi/2$ (hence $\cos\theta > 0$) due to the two assumptions of Case I inflation and upper hemisphere contact. Integrating eq. (34) from the contact edge ($r = a$) to the fixed edge ($r = b$) gives the following result:

$$\int_a^b \frac{1}{\sqrt{r^2 - \left(r^2 - \left(1 + R/R_s\right)a^2\right)^2 / R^2}}\, dr = \ln\frac{b}{\lambda_0 \rho_a}, \tag{35}$$

where ρ_a and b/λ_0 are the material coordinates at the contact edge and fixed edge, respectively. Equation (35) allows us to determine the material coordinate ρ_a for a given contact radius a. Once ρ_a is found, it can be plugged into eq. (31) to determine λ_c, i.e.,

$$\lambda_c = \frac{2a}{\rho_a\left(1 + \sqrt{1 - \left(a/R_s\right)^2}\right)}, \tag{36}$$

which, together with eq. (31), can be used to fully determine the stretch ratios within the contacting membrane.

In summary, during the making contact stage, we have obtained analytical solutions for the membrane profile in eq. (24), the gap d in eq. (25), the contact force F in eq. (26), the material coordinate at the contact edge ρ_a in eq. (35), and the biaxial stretch ratios in the contacting membrane in eqs. (31) and (36), all of which are expressed as functions of the contact radius a and the applied pressure P (through $R = 2\mu h/P$).

3.2 Contact pinning

At the end of the making contact stage, a contact area with radius a_m has been established. The material coordinate ρ_{am} at the contact edge $r = a_m$ can be determined using eq. (35):

$$\rho_{am} = \frac{b}{\lambda_0}\exp\left(-\int_{a_m}^{b}\frac{1}{\sqrt{r^2-\left(r^2-\left(1+R_m/R_s\right)a_m^2\right)^2/R_m^2}}dr\right) \text{ with } R_m = \frac{2\mu h}{P_m}\ , \tag{37}$$

where P_m is the applied pressure at the end of the making contact stage. During the contact pinning stage, G is no longer zero, but is less than W_{ad} so that the membrane is not yet detaching from the substrate. Therefore, the material coordinate of the contact edge remains unchanged during this stage, i.e., $\rho_a = \rho_{am}$, but the contact angle α can be non-zero (see Fig.3b) and the stretch ratio λ_1 can be discontinuous at the contact edge. In particular, the non-contacting membrane can change its shape in response to the external loading (i.e., increasing gap d or decreasing pressure P), leading to an increasing contact angle α. Whether the contact radius a changes or not depends on the tangential boundary condition. Specifically, under the no slip condition, the contacting membrane is locked on the substrate during contact pinning, implying that the contact radius a remains fixed, i.e., $a = a_m$. However, under the frictionless condition, the contacting membrane can slide on the substrate freely and hence can change its stretch in response to the external loading, which can cause changes in the contact radius a. This difference needs to be captured by assigning different boundary conditions at the contact edge as elaborated below.

3.2.1 No slip condition

Under this condition, $\rho_a = \rho_{am}$ and $a = a_m$. The deformed profile of the non-contacting membrane is still governed by eq. (11), but the constants C_1 and C_2 are different from those in eq. (19) for the making contact stage. To determine them, we first note that eqs. (32) and (33) rely

only on the large stretch approximation and are still valid for adhesive contact. Combining eqs. (6) and (32) and knowing that $T_1 > 0$ based on eq. (10), we obtain:

$$\sin\theta = \frac{P\left(r^2 + C_1\right)}{2\sqrt{\mu^2 h^2 r^2 + C_2}} = \frac{r^2 + C_1}{R\sqrt{r^2 + \bar{C}_2}}, \tag{38}$$

where we have defined $\bar{C}_2 = C_2 / \mu^2 h^2$ to simplify notation and used $R = 2\mu h/P$. Right outside the contact edge ($r = a_m$), θ is equal to θ_a which is related to the contact angle α through eq. (22). Applying this boundary condition to eq. (38) and using eq. (22), we have

$$C_1 = \left(\sqrt{1 - \left(\frac{a_m}{R_s}\right)^2}\, \sin\alpha - \frac{a_m}{R_s}\cos\alpha \right) R\sqrt{a_m^2 + \bar{C}_2} - a_m^2 . \tag{39}$$

Another equation is required to solve for the two unknowns C_1 and $\bar{C}_2$. This can be obtained by substituting $\cos^2\theta$ in eq. (33) by $1 - \sin^2\theta$ and using eq. (11), which results in

$$\frac{1}{\sqrt{\left(r^2 + \bar{C}_2\right) - \left(r^2 + C_1\right)^2 / R^2}} \left|\frac{dr}{d\rho}\right| = \frac{1}{\rho}. \tag{40}$$

Integration of eq. (40) from the contact edge ($\rho = \rho_{am}$ and $r = a_m$) to the fixed edge ($\rho = b/\lambda_0$ and $r = b$) can provide an additional equation for C_1 and $\bar{C}_2$. However, we note that $dr/d\rho$ in eq. (40) is not always positive as illustrated in Fig.4. Since the range of contact angle α is from 0 to π, it is possible for θ_a, which is equal to $\alpha - \arcsin\left(a_m / R_s\right)$, to exceed π/2. This results in a negative $\cos\theta_a$, implying that r first decreases from the contact edge until a transition point $r = \eta$ where $\theta = \pi/2$ and then increases to reach the fixed edge ($r = b$) (Fig.4b). Below we consider the two possibilities shown in Fig.4. If $\theta_a \le \pi/2$ (Fig. 4a), $dr/d\rho$ is positive throughout the non-contacting membrane. Therefore, integrating eq. (40) from the contact edge to the fixed edge gives

$$\int_{a_m}^{b} \frac{1}{\sqrt{\left(r^2 + \bar{C}_2\right) - \left(r^2 + C_1\right)^2 / R^2}}\, dr = \ln\rho\Big|_{\rho_{am}}^{\frac{b}{\lambda_0}} = \ln\frac{b}{\lambda_0 \rho_{am}}. \tag{41}$$

If $\theta_a > \pi/2$ (Fig. 4b), $dr/d\rho$ is first negative between $r = \eta$ and $r = a_m$ and then negative between $r = \eta$ and $r = b$, which results in the following equation:

$$\int_{\eta}^{a_m} \frac{1}{\sqrt{\left(r^2+\bar{C}_2\right)-\left(r^2+C_1\right)^2/R^2}}dr+\int_{\eta}^{b} \frac{1}{\sqrt{\left(r^2+\bar{C}_2\right)-\left(r^2+C_1\right)^2/R^2}}dr=\ln\frac{b}{\lambda_0\rho_{am}}. \tag{42}$$

The transition point η can be determined by setting $\theta=\pi/2$ at $r=\eta$ in eq. (38), i.e.,

$$R\sqrt{\eta^2+\bar{C}_2}=\eta^2+C_1, \tag{43}$$

which is essentially a quadratic equation for η^2 and has two possible solutions:

$$\eta^2=\left(\frac{R^2}{2}-C_1\right)\pm\sqrt{\left(\bar{C}_2-C_1\right)R^2+\frac{R^4}{4}}. \tag{44}$$

Since $\eta < a_m$, the solution in eq.(44) that is between 0 and a_m^2 should be selected.

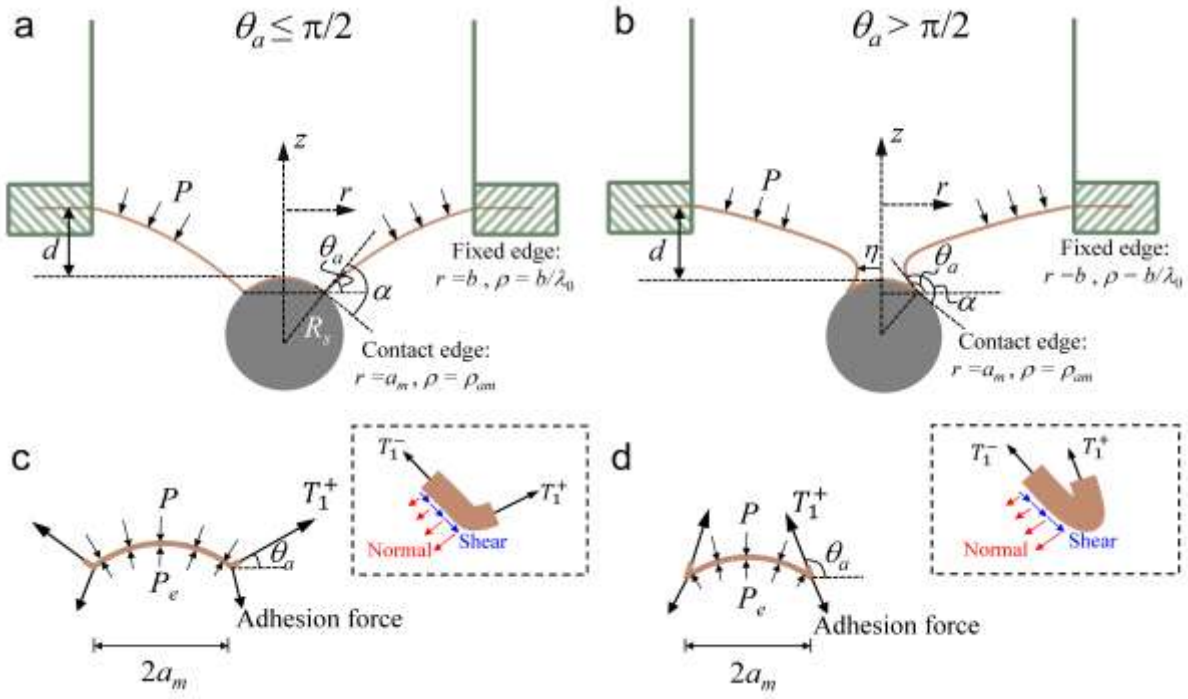

Figure 4. Contact pinning under no slip condition. (a) Membrane profile when $\theta_a \le \pi/2$. Along the non-contacting membrane, the radial coordinate r monotonically increases from the contact edge ($r = a_m$) to the fixed edge ($r = b$). (b) Membrane profile when $\theta_a > \pi/2$. Along the non-contacting membrane, the radial coordinate r first decreases from a_m to η and then increases from η to b. (c-d) Free body diagrams for the contacting membrane (including the contact edge) when (c) $\theta_a \le$

$\pi/2$ and (d) $\theta_a > \pi/2$. The insets show zoomed-in views of the localized normal and shear interface tractions at the contact edge that underlie the concentrated adhesion force.

For a given contact angle α ($0 \le \alpha \le \pi$), the two constants C_1 and $\bar{C}_2$ can be determined using eqs. (39) and (41) when $\alpha \le \pi/2 + \arcsin(a_m/R_s)$ or using eqs. (39) and (42) when $\alpha > \pi/2 + \arcsin(a_m/R_s)$. However, closed-form solutions for C_1 and $\bar{C}_2$ are not available for any α in general. Instead, they need to be solved for numerically. Specifically, one can substitute eq. (39) into eq. (41) or (42) and solve for $\bar{C}_2$ first and then C_1. Once C_1 and $\bar{C}_2$ are determined, we can use the eq. (38) to obtain the following governing equation of the non-contacting membrane profile:

$$\left(\frac{dz}{dr}\right)^2 = \tan^2\theta = \frac{\sin^2\theta}{1-\sin^2\theta} = \frac{\left(r^2+C_1\right)^2}{R^2\left(r^2+\bar{C}_2\right)-\left(r^2+C_1\right)^2}. \tag{45}$$

Integration of eq. (45) depends on θ_a or the contact angle α (i.e., the two cases in Fig.4). If $\theta_a \le \pi/2$ (Fig. 4a), we have

$$z(r) = -\int_r^b \frac{s^2+C_1}{\sqrt{R^2\left(s^2+\bar{C}_2\right)-\left(s^2+C_1\right)^2}}\,ds \quad (a_m \le r \le b). \tag{46}$$

If $\theta_a > \pi/2$ (Fig. 4b), the non-contacting membrane profile is obtained by joining two branches of the $z(r)$ function:

$$z(r) = \begin{cases} -\int_r^b \frac{s^2+C_1}{\sqrt{R^2\left(s^2+\bar{C}_2\right)-\left(s^2+C_1\right)^2}}\,ds & \eta \le r \le b \\ -\int_\eta^r \frac{s^2+C_1}{\sqrt{R^2\left(s^2+\bar{C}_2\right)-\left(s^2+C_1\right)^2}}\,ds - \int_\eta^b \frac{s^2+C_1}{\sqrt{R^2\left(s^2+\bar{C}_2\right)-\left(s^2+C_1\right)^2}}\,ds & \eta < r \le a_m \end{cases}. \tag{47}$$

Using eq. (46) or (47), we can evaluate the gap d (see Fig.4) as

$$d = -z\left(r=a_m\right) - R_s + \sqrt{R_s^2 - a_m^2}. \tag{48}$$

Next we derive the contact force F during contact pinning. Because of adhesion, the contact force F includes two contributions, one from the contact pressure and the other from the adhesive traction on the interface. The adhesive traction should include components that are tangential and normal to the interface. In particular, the tangential component (i.e., interface shear stress) results from the constraint that the contact membrane is locked on the substrate, while the normal component resists separation between the membrane and the substrate (see the insets of Fig.4c-4d). It has been shown in the literature that for a pre-stretched elastic film perfectly bonded to a stiff substrate, the interface traction is localized in a small stress transfer region near the edge of the film, the size of which is on the order of the film thickness (Yu et al., 2001). Given that the membrane thickness h is much smaller than the characteristic length scale of our problem (e.g., contact radius a), we have represented the stress transfer zone as a point at the contact edge, and the adhesive traction as a concentrated adhesion force at the contact edge. Axisymmetry dictates that the two contributions from the contact pressure P_e and the adhesion force result in a net force along the z-axis, which is the contact force F (positive when compressive). Using the free body diagrams shown in Fig.4c-4d and enforcing equilibrium, F is found to be

$$F = \pi a_m^2 P - 2\pi a_m T_1^+ \sin\theta_a , \tag{49}$$

where T_1^+ is the longitudinal line tension right outside the contact edge ($r = a_m$) and can be evaluated using eq. (32), i.e., $T_1^+ = \mu h\sqrt{1+\bar{C}_2 / a_m^2}$. Using this result and eq. (22), we can rewrite eq. (49) as

$$F = \pi P\left[a_m^2 - R\sqrt{a_m^2 + \bar{C}_2}\left(\sqrt{1-\left(\frac{a_m}{R_s}\right)^2}\sin\alpha - \frac{a_m}{R_s}\cos\alpha \right)\right] = -\pi P C_1 , \tag{50}$$

where we have used $R = 2\mu h/P$. A special case worth pointing out is the beginning of contacting pinning when $\alpha = 0$ and $\bar{C}_2 = 0$. Using these values, eq. (50) is reduced to $F = \pi a_m^2 P\left(1 + R / R_s\right)$ which recovers the adhesionless contact solution in eq. (26).

The energy release rate G is expected to increase from 0 during contacting pinning. To evaluate G, we use eq. (23) and implement the large stretch approximation and the equi-baxial condition in the contacting membrane ($\lambda_1^- = \lambda_2$) to obtain:

$$G = T_1^+ \left(1-\cos\alpha\right) + \frac{\mu h}{2}\left(\frac{\lambda_1^+}{\lambda_2} - 1\right)^2 . \tag{51}$$

Since $\lambda_1^+ / \lambda_2 = T_1^+ / \mu h = \sqrt{1+\bar{C}_2 / a_m^2}$, we can further rewrite eq. (51) as

$$\frac{G}{\mu h} = \sqrt{1+\frac{\bar{C}_2}{a_m^2}}\left(1-\cos\alpha\right) + \frac{1}{2}\left(\sqrt{1+\frac{\bar{C}_2}{a_m^2}} - 1\right)^2 . \tag{52}$$

In summary, for contact pinning under the no slip condition, we prescribe the contact angle α and numerically solve the two constants C_1 and $\bar{C}_2$. The membrane profile, gap d, contact force F and energy release rate G can all be computed using analytical solutions given above.

3.2.2 Frictionless condition

Under this condition, adhesion only prevents normal separation of the contacting membrane from the substrate but cannot resist sliding of the contacting membrane on the substrate. Therefore, the contacting membrane can freely adjust its stretch, resulting in a changing contact radius a while the material coordinate of the contact edge ρ_a remains fixed at ρ_{am}. On the other hand, the absence of interface shear traction implies that the adhesion force (see Fig.4c-4d) does not have any component along the tangential direction of the interface, which leads to the following local force balance at the contact edge:

$$T_1^+ \cos\alpha = T_1^- , \tag{53}$$

where T_1^+ and T_1^- are the longitudinal line tension at the contact edge from the non-contacting and contacting parts of the membrane, respectively (see the inset of Fig.3b). Applying the large stretch approximation in eq. (10), we can rewrite eq. (53) as

$$\cos\alpha = \frac{\lambda_2}{\lambda_1^+} = \frac{\mu h}{T_1^+} , \tag{54}$$

where we have used the condition that the contacting membrane is under equal-biaxial stretch ($\lambda_1^- = \lambda_2$) so that $T_1^- = \mu h$. Equation (54) implies that the contact angle $\alpha < \pi/2$ so that $\cos\alpha > 0$,

otherwise the tangential force balance in eq. (53) cannot be satisfied. This is different from the no slip condition where α can exceed $\pi/2$. The line tension T_1^+ can be determined by applying eq. (32) at the contact edge ($r = a$), based on which we can rewrite eq. (54) as

$$\bar{C}_2 = a^2 \tan^2 \alpha \,. \tag{55}$$

To solve for C_1, we substitute eq. (55) into eq. (38) and utilize $\theta(r = a) = \theta_a$ and $\cos\alpha > 0$, which gives

$$C_1 = \frac{aR\sin\theta_a}{\cos\alpha} - a^2 = aR\sqrt{1-\left(\frac{a}{R_s}\right)^2}\tan\alpha - \left(1+\frac{R}{R_s}\right)a^2, \tag{56}$$

where we have used eq. (22) to relate θ_a and α. Unlike the no slip solution where the contact radius is fixed during contact pinning, here the contact radius a can change as the contact angle α increases. To determine a, we note that eq. (40) is still valid for the non-contacting membrane and the material coordinate at the contact edge remains at ρ_{am}. Since here $\alpha < \pi/2$, we conclude that $\theta_a < \pi/2$, implying $dr/d\rho > 0$ for the non-contacting membrane, i.e., only the scenario in Fig.4a is possible for the frictionless condition. Using this condition and integrating eq. (40) from the contact edge ($\rho = \rho_{am}$ and $r = a$) to the fixed edge ($\rho = b/\lambda_0$ and $r = b$), we obtain

$$\int_a^b \frac{1}{\sqrt{\left(r^2 + a^2\tan^2\alpha\right) - \left(r^2 + aR\sqrt{1-\left(a/R_s\right)^2}\tan\alpha - \left(1+R/R_s\right)a^2\right)^2 / R^2}}\,dr = \ln\frac{b}{\lambda_0\rho_{am}}, \tag{57}$$

where ρ_{am} is given by eq. (37) and we have substituted $\bar{C}_2$ and C_1 using eq. (55) and (56), respectively. Equation (57) allows us to determine the contact radius a numerically for a given contact angle α. After that, the $\bar{C}_2$ and C_1 can be readily calculated, and hence the profile of the non-contacting membrane can be determined using eq. (46) except that the range of r should be changed to $a \le r \le b$. The gap d is evaluated using the $z(r)$ function in eq. (46):

$$d = -z\left(r = a\right) - R_s + \sqrt{R_s^2 - a^2}\,. \tag{58}$$

Similar to Section 3.2.1, the contact force F and energy release rate G are still respectively given by eq. (49) and (51) except that the contact radius a_m should be replaced by a. Here since $T_1^+ = \mu h / \cos\alpha$, the contact force F can be further simplified to

$$F = \pi P \left[\left(1 + \frac{R}{R_s} \right) a^2 - aR \sqrt{1 - \left(\frac{a}{R_s} \right)^2} \tan\alpha \right] = -\pi P C_1 . \tag{59}$$

The energy release rate G is

$$\frac{G}{\mu h} = \frac{1 - \cos\alpha}{\cos\alpha} + \frac{1}{2} \left(\frac{1}{\cos\alpha} - 1 \right)^2 = \frac{\tan^2\alpha}{2} . \tag{60}$$

Interestingly, eq. (60) shows that G approaches $+\infty$ as α approaches $\pi/2$, consistent with the constraint $\alpha < \pi/2$ from eq. (54).

In summary, for contact pinning under the frictionless condition, we prescribe the contact angle α, numerically determine the contact radius a from eq. (57) and then calculate the two constants C_1 and $\bar{C}_2$. The membrane profile, gap d, contact force F and energy release rate G can all be computed using analytical solutions derived in this section.

3.3 Delamination

The contact pinning stage ends when the energy release rate G reaches the work of adhesion W_{ad}. After that the contacting membrane starts to be detached from the substrate. Consequently, the material coordinate of the contact edge, denoted as ρ_{ad}, is smaller than its counterpart ρ_{am} during contact pinning and continues to decrease during delamination. Therefore, in this stage we solve for the membrane deformation under a given ρ_{ad} ($0 \le \rho_{ad} \le \rho_{am}$). The contact angle α is no longer prescribed, but is rather determined from the equilibrium equation for quasi-static delamination: $G = W_{ad}$. Most of the analytical solutions in Section 3.2 can still be applied for this stage as detailed below.

3.3.1 No slip condition

Under the no slip condition, the membrane in the contact region ($0 \le \rho \le \rho_{ad}$) remains fixed on the substrate. Therefore, we can determine the contact radius a_d corresponding to ρ_{ad} using the deformation field established in the making contact stage (Section 3.1). Specifically, a_d and ρ_{ad} can be identified as r^* and ρ^* in eq. (31). Moreover, using eq. (36) to substitute λ_c, we obtain

$$\frac{\rho_{ad}}{\rho_{am}} = \frac{a_d}{a_m} \frac{1+\sqrt{1-\left(a_m / R_s\right)^2}}{1+\sqrt{1-\left(a_d / R_s\right)^2}}. \tag{61}$$

The contact pinning solutions in Section 3.2.1 can be applied here provided that ρ_{am} and a_m are replaced by ρ_{ad} and a_d, respectively. However, the contact angle α is not given and needs to satisfy the condition $G = W_{ad}$. Using eq. (52) and replacing a_m by a_d, we have

$$\frac{W_{ad}}{\mu h} = \sqrt{1+\frac{\bar{C}_2}{a_d^2}}\left(1-\cos\alpha\right) + \frac{1}{2}\left(\sqrt{1+\frac{\bar{C}_2}{a_d^2}}-1\right)^2. \tag{62}$$

With eq. (62), we can solve for α through an iterative process. Specifically, for a set of given ρ_{ad} and a_d, we start with an initial guess of α and follow the procedures outlined in Section 3.2.1 to solve for C_1 and $\bar{C}_2$ with ρ_{am} and a_m replaced by ρ_{ad} and a_d. The resulting $\bar{C}_2$, together with α and a_d, are then substituted into the right hand side of eq. (62) to test whether this equation is satisfied. If not, α is adjusted iteratively until eq. (62) is satisfied. Once α and the corresponding C_1 and $\bar{C}_2$ are determined, we follow eqs. (48) and (50) to determine the gap d and contact force F with a_m replaced by a_d.

3.3.2 Frictionless condition

Under the frictionless condition, the contact radius α corresponding to ρ_{ad} is not known. However, eq. (60) shows that the energy release rate G depends only on the contact angle α. Since $G = W_{ad}$ during the delamination stage, we expect a constant contact angle given by

$$\alpha = \arctan\sqrt{\frac{2W_{ad}}{\mu h}}, \qquad (0 \le \alpha < \pi/2). \tag{63}$$

Using this contact angle α, we can solve for the contact radius a from eq. (57) with ρ_{am} replaced by ρ_{ad}. After that, the constants C_1 and $\bar{C}_2$, the gap d, and the contact force F can be determined from eqs. (56), (55), (58) and (59), respectively.

4. Finite Element Analysis

We developed an axisymmetric Finite Element Analysis (FEA) model using a commercial software package ABAQUS (version 2021, Simulia, Providence, RI) to simulate the inflation of a neo-Hookean membrane and its contact with and delamination from a rigid substrate. The FEA model is capable of simulating the contact mechanics between the inflated membrane and substrates with different curvatures and adhesive interactions. Below we briefly describe the FEA model and the simulation procedures. Since the purpose of the FEA model is to provide independent results for comparison with our analytical model, we have only shown selected FEA results in Section 5 and the corresponding model parameters are specified below.

The membrane in its undeformed state is a circular sheet with a radius of $\beta = b/\lambda_0 = 1$ mm and a thickness of $h = 1$ μm. It is modeled as an axisymmetric, deformable part and is meshed using the two-node axisymmetric shell elements (SAX1) with a uniform mesh size of 2 μm. The material model adopted for the membrane is the incompressible neo-Hookean solid with a shear modulus of $\mu = 2$ MPa. The spherically curved substrate with a radius of $R_s = 1$ mm was modeled using an axisymmetric, analytically rigid wire which does not require meshing. Centers of the membrane and the substrate are both placed on the axis of symmetry. To simulate adhesion between the membrane and the substrate, we use the cohesive interaction feature in ABAQUS defined by a damage initiation criterion driven by the maximum interfacial stress and a damage evolution rule based on the energy release rate. We have used a maximum interface stress of $\sigma_{max} = 50$ kPa and a work of adhesion of $W_{ad} = 0.4$ J/m^2 for the cohesive interaction. The two limiting cases of tangential interface behaviors, no slip and frictionless conditions, are modeled by choosing specific initial stiffness coefficients K of the cohesive traction-separation relation, i.e., isotropic ($K_{nn} = K_{ss} = K_{tt}$) for the no slip condition and zero-shear ($K_{ss} = K_{tt} = 0$) for the frictionless condition, where the subscript n represents the normal direction of the interface and the subscripts s and t represent the two tangential directions of the interface.

Each simulation consists of three steps. First, an equi-biaxial planar stretch of $\lambda_0 = 2$ is applied to the membrane so that its radius becomes $b = 2$ mm. Second, the membrane is inflated and makes contact with the substrate. This is achieved either by inflating the membrane to a pressure P and then reducing its gap with the substrate with the pressure kept constant or by moving the substrate to a certain gap d below the membrane and then inflating the membrane under an increasing pressure. The former loading method will be referred to as displacement control, and the latter will be referred to as pressure control. During this step, the contact between the membrane and the substrate is effectively adhesionless, because the cohesive interaction defined above is not activated until a contact interface is established and thus does not provide any adhesive tractions when the contact radius is increasing. Third, the last step simulates the contact pinning and delamination stages, which is achieved by increasing the gap with the pressure kept constant (displacement control) or reducing the applied pressure with the gap kept constant (pressure control). During this step, the cohesive interaction can provide adhesive tractions across the contact interface to resist separation. The external loadings, i.e., pressure and displacement, are applied following a linear ramp. The first step (pre-stretch) and the second step (inflation and making contact) are carried out using the Static solver of ABAQUS. For the third step (contact pinning and delamination), to aid numerical convergence we switch to the Dynamic/Implicit solver. Results for the contact force, contact displacement and applied pressure are extracted from the FEA simulations and compared with those from the analytical model for validation.

5. Results and Discussions

In this section we illustrate results of our analytical model for the three stages of membrane contact. To facilitate discussion, we first categorize the parameters of our analytical model into two types: i) loading parameters that vary during the contact process: applied pressure P, gap d (or contact displacement δ), contact force F and contact radius a; ii) system parameters that remain constant during the contact process: pre-stretch λ_0, membrane stiffness μh, membrane radius b, substrate radius R_s, work of adhesion W_{ad}, the maximum contact radius a_m achieved after the making contact stage and the corresponding material coordinate ρ_{am}. With a set of prescribed system parameters, our analytical model can provide solutions relating the loading parameters. Specifically, we consider two experimentally motivated scenarios of membrane contact:

displacement control (Section 5.1) and pressure control (Section 5.2), where the contact process is implemented by controlling the gap d under a fixed pressure P or controlling the pressure P under a fixed gap d, respectively. In both scenarios, our focus is on calculating the contact force F (positive when compressive) since it is typically measureable in experiments.

To reduce the number of independent variables, we set the pre-stretch at $\lambda_0 = 2$ and normalize the loading and system parameters using the membrane stiffness μh and the radius b. For example, the normalized pressure is $Pb/2\mu h$, where the factor 2 is motivated by the fact that $2\mu h/P$ is the free inflation radius R and hence $Pb/2\mu h$ can be interpreted as b/R. Accordingly, the other parameters are normalized as follows: gap d/b, contact displacement δ/b, contact force $F/2\mu hb$, substrate radius R_s/b, work of adhesion $W_{ad}/\mu h$, and the maximum contact radius a_m/b.

5.1 Displacement control

Under displacement control the inflated membrane is essentially a spherical adhesive probe with a radius of $R = 2\mu h/P$. Here our goal is to obtain the contact force F as a function of the contact displacement δ. The making contact stage is analogous to the Hertzian contact between an elastic sphere and a rigid sphere, except that here the elastic sphere is replaced by the inflated membrane (i.e., a hollow spherical probe). In this stage, we first prescribe a contact radius a in the range of $0 \le a \le a_m$ and use eqs. (24), (25) and (26) to determine the membrane profile, gap d and contact force F, respectively. Since the applied pressure is fixed at P, the P_m in eq. (37) is now equal to P.

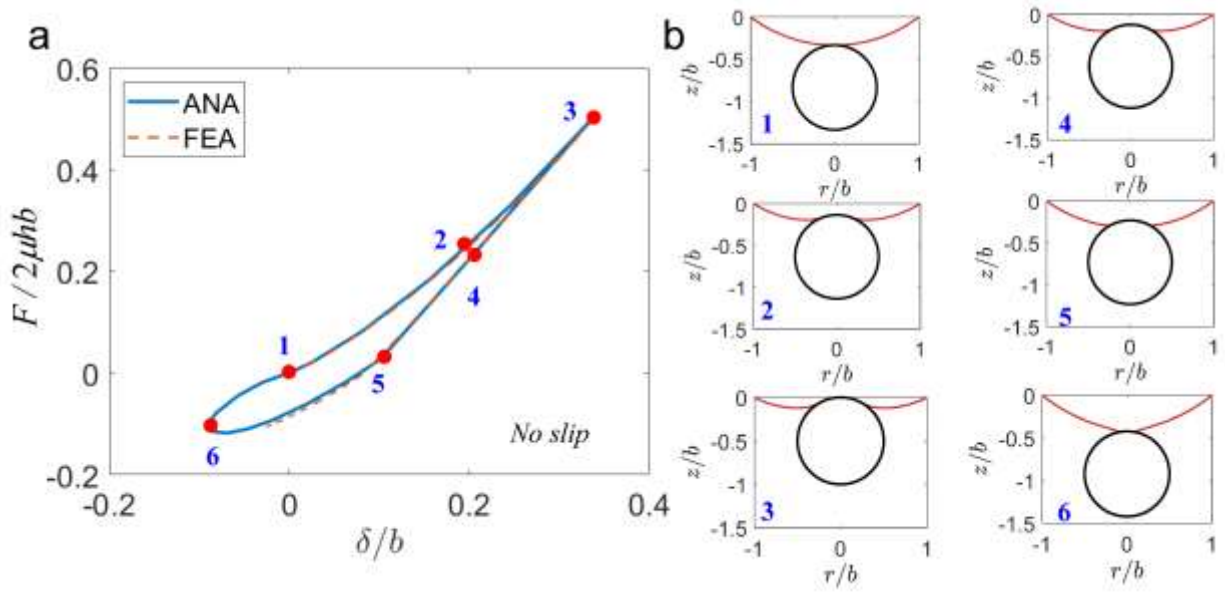

Figure 5. Representative results for membrane contact under displacement control with no slip condition. (a) Normalized contact force $F/2\mu hb$ versus normalized contact displacement δ/b. The solid line ("ANA") is obtained using our analytical model and the dashed line ("FEA") represents the FEA result. (b) Deformation profiles of the membrane at six different points in (a). The parameters used are $Pb/2\mu h = 0.6$, $W_{ad}/\mu h = 0.2$, $R_s/b = 0.5$ and $a_m/b = 0.25$.

Results for the stages of contact pinning and delamination depend on whether the no slip or frictionless condition is adopted. We first consider the no slip condition. During contact pinning, we gradually increase the contact angle α from 0. For a given α, we follow the procedures described in Section 3.2.1 to solve for the two constants C_1 and $\bar{C}_2$, and then the membrane profile, gap d and contact force F using eq. (46) or (47), eq. (48) and eq. (50), respectively. Meanwhile, the energy release rate G for any given α is determined using eq. (52). When G becomes equal to W_{ad}, the delamination stage begins. During delamination, the contact angle α cannot be prescribed. Instead, we gradually change the contact radius a_d from a_m to 0 and use eq. (62) to solve for the corresponding contact angle α, after which the membrane profile, gap d and contact force F can be determined following the procedures described in Section 3.3.1. A representative result is shown in Fig. 5a where the contact force F (positive when compressive) is plotted as a function of the contact displacement δ calculated from the gap d using eq. (21). The membrane profiles at six

different points along the F-δ curve are shown in Fig. 5b. Also plotted in Fig. 5a is the F-δ curve obtained from FEA simulation, which agrees well with our analytical model. Interestingly, despite that our solutions are obtained based on the nonlinear neo-Hookean membrane model, the F-δ relation during contact pinning (Point 3 to 5) is approximately linear, indicating a constant contact stiffness during this stage. Note that the FEA result does not cover the entire delamination stage (Point 5 to Point 6 and Point 1) due to convergence difficulties. In contrast, the analytical model is capable of providing a full solution for the delamination stage.

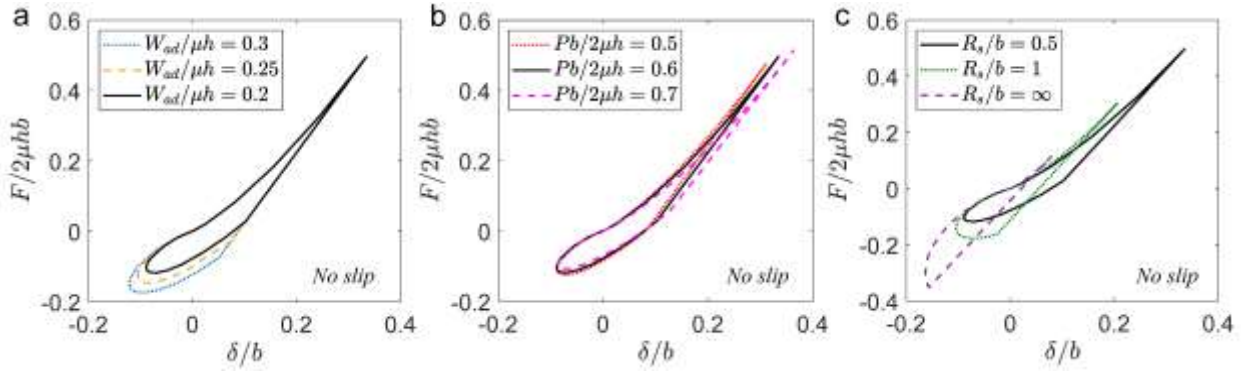

Figure 6. Parametric study for membrane contact under displacement control with no slip condition. (a) Effect of adhesion $W_{ad}/\mu h$ with $Pb/2\mu h$ = 0.6 and R_s/b = 0.5. (b) Effect of applied pressure $Pb/2\mu h$ with $W_{ad}/\mu h$ = 0.2 and R_s/b = 0.5. (c) Effect of substrate radius R_s/b with $W_{ad}/\mu h$ = 0.2 and $Pb/2\mu h$ = 0.6. For all results we have used a_m/b = 0.25.

The analytical model allows us to perform a parametric study efficiently, as demonstrated in Fig.6 where we show how the work of adhesion $W_{ad}/\mu h$, applied pressure $Pb/2\mu h$ and substrate radius R_s/b affect the contact process. Specifically, Fig.6a shows that the work of adhesion W_{ad} does not affect the stage of making contact and the stiffness (i.e., the slope of F-δ curve) during contact pinning but can increase the pull-off force (i.e., the most negative value of F during delamination). This is expected since W_{ad} determines only when the delamination stage is initiated and how it progresses. Figure 6b shows the effect of applied pressure P: a higher P tends to decrease the contact stiffness, as reflected in the smaller slope of the F-δ curve, and reduce the pull-off force. This trend is attributed to the smaller free inflation radius R (= $2\mu h/P$) under a higher

pressure P. Finally, Fig.6c shows that a larger substrate radius R_s tends to increase the contact stiffness and pull-off force. Note that the limiting case of $R_s/b = \infty$ represents a flat substrate.

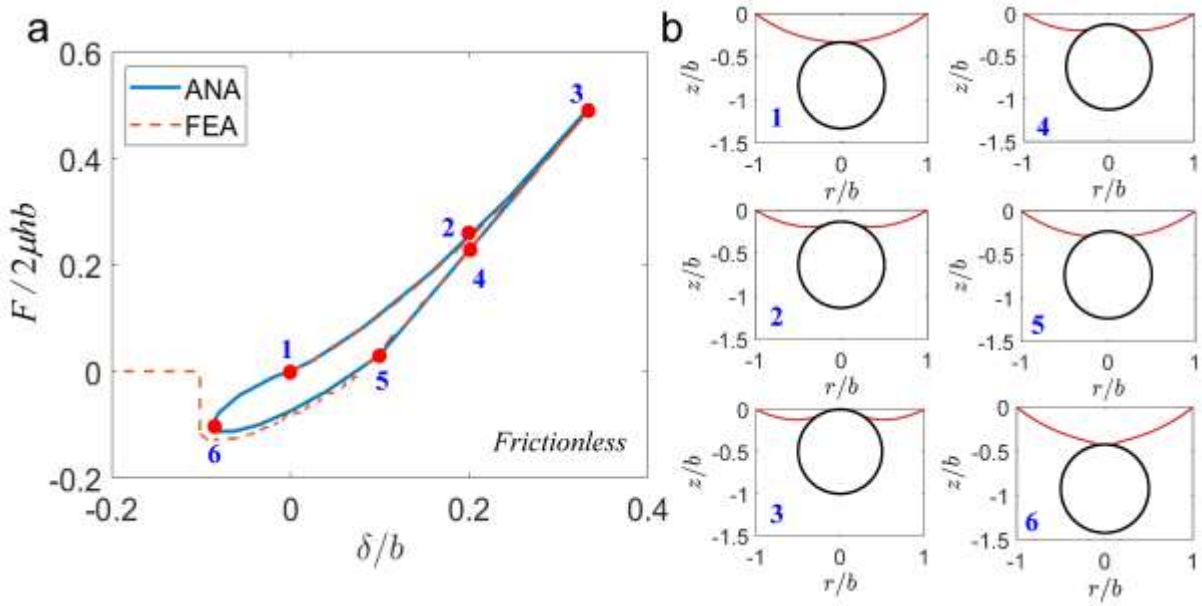

Figure 7. Representative results for membrane contact under displacement control with frictionless condition. (a) Normalized contact force $F/2\mu hb$ versus normalized contact displacement δ/b. The solid line ("ANA") is obtained using our analytical model and the dashed line ("FEA") represents the FEA result. (b) Deformation profiles of the membrane at six different points in (a). The parameters used are $Pb/2\mu h = 0.6$, $W_{ad}/\mu h = 0.2$, $R_s/b = 0.5$ and $a_m/b = 0.25$.

Next we consider the frictionless condition. During contact pinning, for a given α, we first solve for the contact radius a using eq. (57), based on which the two constants C_1 and $\bar{C}_2$ can be determined using eqs. (56) and (55). With the values of C_1 and $\bar{C}_2$, the membrane profile, gap d and contact force F are calculated using eq. (46) (with a_m replaced by a), eq. (58) and eq. (59), respectively. Since the energy release rate G is directly related to the contact angle α through eq. (60), we can easily determine when the delamination stage begins as G reaches W_{ad}. During delamination, eq. (63) suggests that the contact angle is a constant, which greatly simplifies the solution process. Specifically, during delamination we prescribe the material coordinate of the contact edge ρ_{ad} ($0 \le \rho_{ad} \le \rho_{am}$) and follow the procedures described in Section 3.3.2 to determine

the membrane profile, gap d and contact force F. A representative result is shown in Fig. 7a in terms of the F-δ curve with the corresponding membrane profiles given in Fig.7b. The shape of the F-δ curve in Fig.7a closely resembles that for the no slip condition (see Fig.5a), but quantitative comparison reveals that the frictionless condition leads to slight decreases in the contact stiffness and pull-off force. The FEA result shown in Fig.7a is obtained using the zero-shear setting for the cohesive interaction (see Section 4) and agrees well with the analytical model except near the end of delamination (i.e., beyond Point 6 in Fig.7a). This discrepancy is due to the displacement controlled loading in the FEA simulation, i.e., the delamination stage is simulated by monotonically decreasing the contact displacement δ (or increasing the gap d). As a result, the segment from Point 6 to Point 1 in Fig.7a is not accessible to the FEA simulation. Instead, we observe a sudden pull-off in the FEA simulation where the contact radius jumps to zero when the minimum contact displacement (or the maximum gap) is achieved. This pull-off behavior is essentially the onset of unstable interface crack propagation and is similar to that found in the JKR theory (Johnson and Greenwood, 2013). In experiments the point of pull-off also depends on the compliance of the loading device (Johnson and Greenwood, 2013). We also performed a parametric study for the frictionless condition. The results, illustrated in Fig.8, show similar trends as those observed for the no slip condition (see Fig.6). It is worth noting that the difference caused by the no-slip and frictionless conditions is overall small but becomes more pronounced for the flat substrate (see the case of $R_s/b = \infty$ in Fig.6c and Fig.8c).

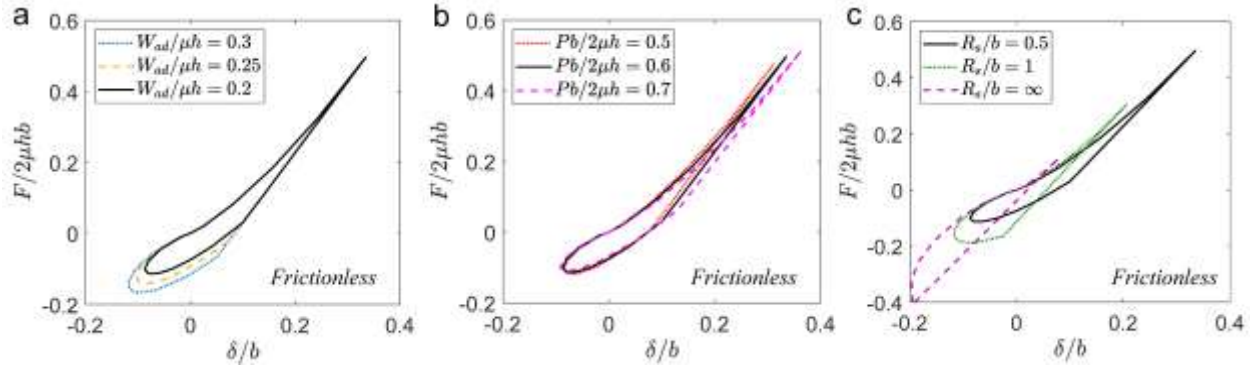

Figure 8. Parametric study for membrane contact under displacement control with frictionless condition. (a) Effect of adhesion $W_{ad}/\mu h$ with $Pb/2\mu h = 0.6$ and $R_s/b = 0.5$. (b) Effect of applied pressure $Pb/2\mu h$ with $W_{ad}/\mu h = 0.2$ and $R_s/b = 0.5$. (c) Effect of substrate radius R_s/b with $W_{ad}/\mu h = 0.2$ and $Pb/2\mu h = 0.6$. For all results we have used $a_m/b = 0.25$.

5.2 Pressure control

The scenario of pressure control is motivated by experimental works that used an inflated membrane for adhesion measurement (Flory et al., 2007; Laprade et al., 2013). In this scenario, the pre-stretched membrane is placed at a fixed gap d above the substrate. The process of making contact and delamination is implemented by increasing and decreasing the pressure P. Similar to Section 5.1, our goal here is to compute the contact force F as the applied pressure P changes. To start the making contact stage, the pressure P should exceed a critical value P_{cr} at which the membrane deflection under free inflation (i.e., d_0 in eq. (15)) is equal to the fixed gap d, since this is the point where the apex of the inflated membrane first reaches the top of the substrate. Using eq. (15), we find the normalized critical pressure $P_{cr}b/2\mu h$ to be:

$$\frac{P_{cr}b}{2\mu h} = \frac{2(d/b)}{(d/b)^2+1}. \tag{64}$$

Recall that in this work we focus on the Case I solution of free inflation (see Fig.2b), which imposes an upper limit for the gap, i.e., $d \le b$. Under this constraint, P_{cr} is an increasing function of d. Note that it is possible for d to be negative. In this case, a negative P_{cr} is needed to maintain point contact between the membrane and the substrate. When solving for the making contact stage, we prescribe a contact radius a ($0 \le a \le a_m$) and numerically solve the pressure P ($P \ge P_{cr}$) from eq. (25) to match the given fixed gap d. After that the membrane profile and contact force F are calculated using eqs. (24) and (26), respectively.

The contact pinning and delamination stages depend on whether the no slip or frictionless condition is assumed. We first consider the no slip condition. During contact pinning, we gradually decrease the pressure P from P_m (i.e., the applied pressure at the end of the making contact stage). For each prescribed P, we assume a contact angle α, solve for the two constants C_1 and $\bar{C}_2$, and examine whether eq. (48) is satisfied with the fixed gap d. This allows us to iteratively determine the contact angle α needed to enforce constant gap d under a decreasing pressure P. Once α is determined, the membrane profile, contact force F and energy release rate G can be calculated using eq. (46) or (47), eq. (50) and eq. (52), respectively. The delamination stage starts when $G = W_{ad}$. During delamination, we prescribe a contact radius a_d ranging from a_m to 0 and numerically solve for the contact angle α and the pressure P to enforce eq. (62) and the constant gap d, after which the membrane profile and contact force F can be determined accordingly following Section

3.3.1. A representative result is shown in Fig. 9a where the contact force F is plotted as a function of the pressure P. The membrane profiles at six different points along the F-δ curve are shown in Fig. 9b. For this example, the fixed gap $d = 0$, indicating that the flat, pre-stretched membrane is already in point contact with the top of the substrate (see membrane profile at Point 1 in Fig.9b). As a result, the contact force F starts to increase as soon as the pressure P is larger than zero. Interestingly, the F-P curve in Fig.9a has a similar shape as the F-d curve in Fig.5a, despite the distinct scenarios of load control. The FEA result shown in Fig.9a also agrees well with our analytical model.

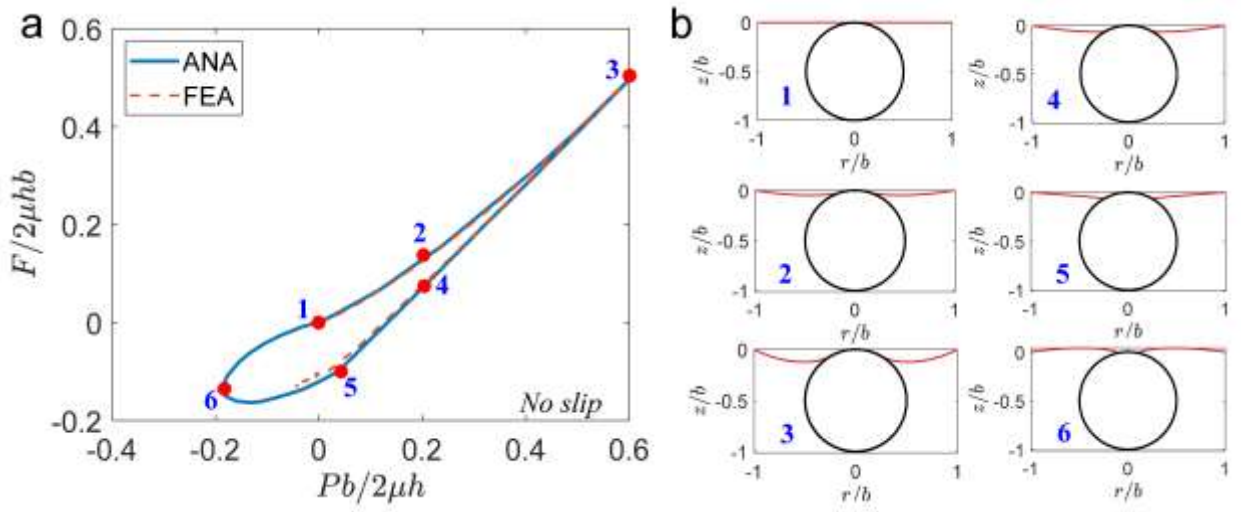

Figure 9. Representative results for membrane contact under pressure control with no slip condition. (a) Normalized contact force $F/2\mu hb$ versus normalized applied pressure $Pb/2\mu h$. The solid line ("ANA") is obtained using our analytical model and the dashed line ("FEA") represents the FEA result. (b) Deformation profiles of the membrane at six different points in (a). The parameters used are $d/b = 0$, $W_{ad}/\mu h = 0.2$, $R_s/b = 0.5$ and $a_m/b = 0.25$.

Figure 10 shows the F-P curves obtained using different parameters. While effects of the work of adhesion $W_{ad}/\mu h$ (Fig. 10a) and substrate radius R_s/b (Fig. 10c) are similar to those observed for displacement control (Fig. 6), the effect of the fixed gap d is more interesting. Increasing d clearly shifts the F-P curve to the right, which is expected since larger d implies that a higher pressure is needed to bring the membrane into contact with the substrate. Apart from the shift, increasing d

also results in higher contact force to achieve the same contact radius during making contact but reduces the pull-off force during delamination.

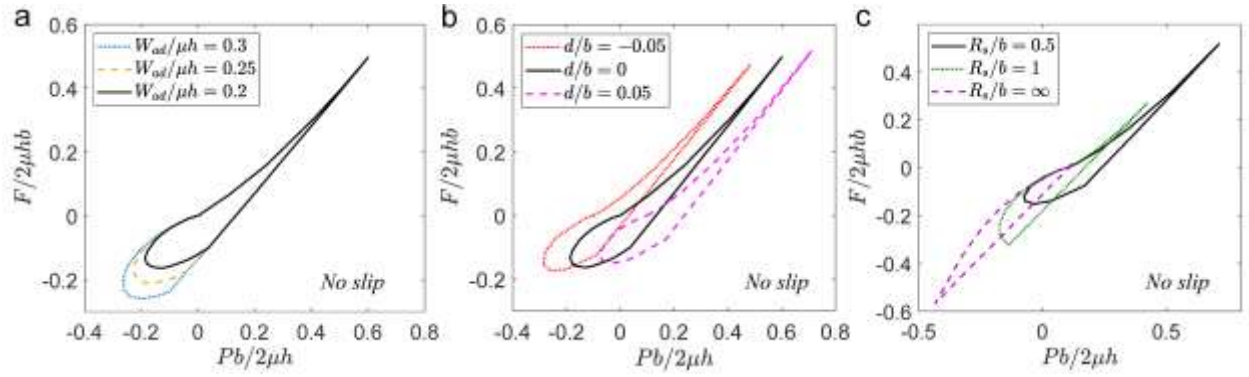

Figure 10. Parametric study for membrane contact under pressure control with no slip condition. (a) Effect of adhesion $W_{ad}/\mu h$ with $d/b = 0$ and $R_s/b = 0.5$. (b) Effect of gap d/b with $W_{ad}/\mu h = 0.2$ and $R_s/b = 0.5$. (c) Effect of substrate radius R_s/b with $W_{ad}/\mu h = 0.2$ and $d/b = 0$. For all results we have used $a_m/b = 0.25$.

Next we consider the frictionless condition. During contact pinning, for a given pressure P ($P \leq P_m$), we iteratively solve for the contact angle α by calculating the contact radius a from eq. (57) and examining if the gap d is equal to the given value. Once α is determined, the membrane profile, contact force F and energy release rate G are calculated using eq. (46) (with a_m replaced by a) and eq. (59) and eq. (60), respectively. When $G = W_{ad}$, the delamination stage starts during which the contact angle α is a constant according to eq. (63). Therefore, we prescribe the material coordinate of the contact edge ρ_{ad} ($0 \leq \rho_{ad} \leq \rho_{am}$) and solve for the pressure P required to enforce the fixed gap, after which the membrane profile and contact force F can be determined following Section 3.3.2. A representative result is shown in Fig. 11a in terms of the F-P curve with the corresponding membrane profiles given in Fig.11b. Again, the shape of the F-P curve in Fig.11a resembles that for the no slip condition (see Fig.9a), but the frictionless condition decreases the pull-off force slightly. The FEA result shown in Fig.11a agrees well with the analytical model except that it cannot capture the unstable segment from Point 6 and Point 1 and exhibits a pull-off behavior instead (similar to the FEA result in Fig.7a). Results of the parametric study in Fig.12 exhibit similar trends as those observed for the no slip condition (see Fig.10).

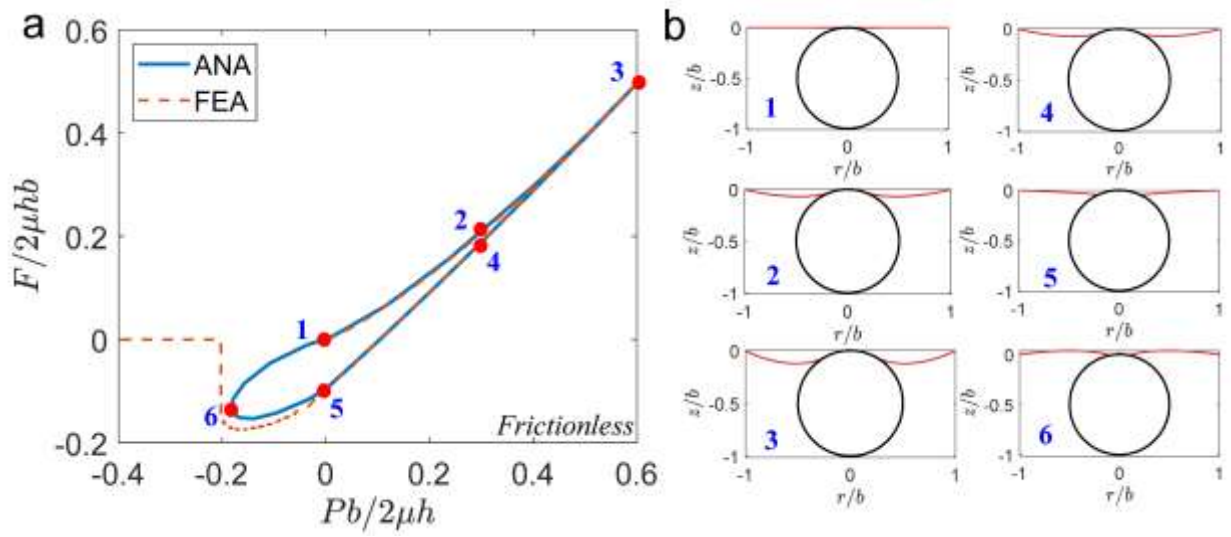

Figure 11. Representative results for membrane contact under pressure control with frictionless condition. (a) Normalized contact force $F/2\mu hb$ versus normalized applied pressure $Pb/2\mu h$. The solid line ("ANA") is obtained using our analytical model and the dashed line ("FEA") represents the FEA result. (b) Deformation profiles of the membrane at six different points in (a). The parameters used are $d/b = 0$, $W_{ad}/\mu h = 0.2$, $R_s/b = 0.5$ and $a_m/b = 0.25$.

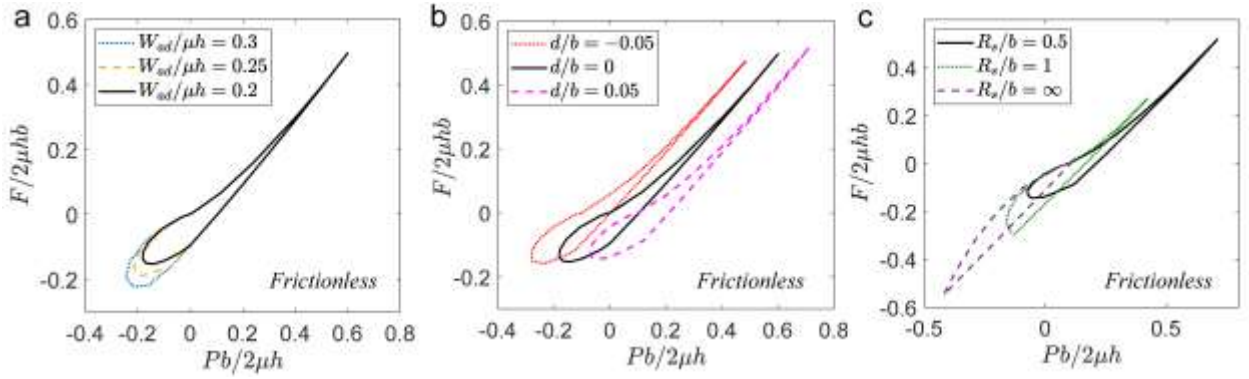

Figure 12. Parametric study for membrane contact under pressure control with frictionless condition. (a) Effect of adhesion $W_{ad}/\mu h$ with $d/b = 0$ and $R_s/b = 0.5$. (b) Effect of gap d/b with $W_{ad}/\mu h = 0.2$ and $R_s/b = 0.5$. (c) Effect of substrate radius R_s/b with $W_{ad}/\mu h = 0.2$ and $d/b = 0$. For all results we have used $a_m/b = 0.25$.

5.3 Discussion

The results presented in Sections 5.1-5.2 demonstrate the utility of our analytical model. These results are based on a number of assumptions in addition to the large stretch approximation for the neo-Hookean solid (see eq. (10)). Here we summarize and discuss these assumptions since they are instrumental for understanding the applicability range of our model.

First, we assumed two scenarios of loading, i.e., displacement control with fixed pressure and pressure control with fixed gap. While both scenarios can be implemented experimentally, there are other loading scenarios. For example, in the experiment of Song et al. (2019), an initially flat circular membrane was first brought into contact with a spherical substrate under a preload. After that a negative pressure was applied on the membrane by a syringe pump and then the membrane was retracted from the substrate with the syringe pump held fixed. During the retraction process, the pressure on the membrane was not constant. Instead, the amount of air within the space enclosed by the membrane, the syringe, and the tube connecting them was held constant. As a result, during retraction the pressure decreased as the membrane underwent deformation and increased its enclosed volume. Our analytical model can be adapted to this loading scenario. Specifically, the preload process can be modeled using the making contact stage (Section 3.1) with displacement control and zero pressure. For the retraction, we can use solutions for the contact pinning and delamination stages (Section 3.2 and 3.3) under displacement control. However, the pressure P is not prescribed but should be obtained by enforcing the ideal gas law that the pressure in the system (membrane, syringe, and tube) multiplied by the system volume is a constant. Note that the pressure P in our analytical model is the pressure differential across the membrane and hence is equal to the system pressure minus the atmospheric pressure.

Second, we have followed eq. (23) derived in Long et al. (2010) to determine the energy release rate G. This energy release rate is defined with respect to the deformed membrane area, i.e., it is the energy released per unit area of deformed membrane detached from the substrate. Accordingly, the work of adhesion W_{ad} is also defined with respect to the deformed membrane area. Alternatively, the energy release rate can be defined with respect to the undeformed reference configuration of the membrane as in Begley et al. (2013). This definition, denoted as G^{un}, is different from ours if the membrane undergoes large biaxial stretch. For the axisymmetric geometry considered in this work, G and G^{un} are related through $G^{un} = \lambda_1^{-}\lambda_2 G$ since $\lambda_1^{-}\lambda_2$ is the

areal stretch ratio at the contact edge (Long et al., 2010). The work of adhesion corresponding to G^{un}, denoted as W_{ad}^{un}, is the energy required to detach a unit undeformed area of the membrane from the substrate. Our analytical model can be readily modified to be in terms of G^{un} and W_{ad}^{un} by using $G^{un} = \lambda_1^- \lambda_2 G$. The two approaches of modeling adhesion are equivalent if we set $W_{ad}^{un} = \lambda_1^- \lambda_2 W_{ad}$. However, since $\lambda_1^- \lambda_2$ is not a fixed value but varies with membrane deformation, we can only assume one of W_{ad}^{un} and W_{ad} to be constant, which should depend on the nature of adhesive interaction on the contact interface. An implicit assumption in our analytical model is that W_{ad} defined with respect to the deformed membrane area is a constant parameter.

Third, we considered two limiting cases of tangential interface behavior: no slip and frictionless. The solution for the frictionless condition is simpler. However, the results presented in Sections 5.1 and 5.2 show that these two cases do not result in any qualitative difference. Quantitatively, the frictionless solution resulted in slightly smaller pull-off forces than the no slip solution. Therefore, for simplicity the frictionless solution could be adopted. It is worth noting that the frictionless solution here is analogous to the JKR theory for the adhesive contact between two elastic spheres where any frictional tractions on the contact interface are neglected and only normal tractions are considered.

Finally, we assumed Hertzian contact (i.e., adhesionless and frictionless) during the making contact stage (see Section 2.1). If this is not the case, the making contact stage can also be assigned a work of adhesion W_{ad}^*, which is typically smaller than the W_{ad} during delamination (Shull, 2002; Vajpayee et al., 2008). Accordingly, we need to enforce $G = W_{ad}^*$ and consider the no slip or frictionless condition during the making contact stage. For the no slip condition, one can follow similar procedures in Section 3.3.1 with W_{ad} replaced by W_{ad}^*. Also, since we can no longer use eq. (61) to relate a_d and ρ_{ad}, we would need to gradually increase the contact radius a and incrementally solve for the stretch distribution within the contact area and the material coordinate of the contact edge ρ_a. In contrast, the frictionless condition is easier, since eq. (63) allows us to prescribe a non-zero contact angle during the making contact stage: $\alpha = \arctan\sqrt{2W_{ad}^* / \mu h}$. This implies that we can gradually increase the contact radius a, and directly calculate C_1 and $\bar{C}_2$ using

eqs. (56) and (55) for the making contact stage. The material coordinate of the contact edge ρ_a can be determined by solving eq. (57) with ρ_{am} replaced by ρ_a.

6. Conclusions

We developed an analytical model to describe the adhesive contact mechanics of an inflated neo-Hookean membrane with a spherically curved, rigid substrate. The entire contact process was divided into three stages: making contact, contact pinning and delamination. Among them, the making contact stage was assumed to be subjected to Hertzian contact (i.e., adhesionless and frictionless), while the contact pinning and delamination stages were under adhesive contact with either no slip or frictionless condition for the tangential interface behavior. Using the large stretch approximation for the neo-Hookean membrane, we obtained analytical expressions relating the membrane profile, contact force F and contact displacement δ to the contact radius a, applied pressure P, work of adhesion W_{ad} and other system parameters. Solutions of our analytical model were found to agree well with results from independent FEA simulations. We also found that the frictionless condition resulted in simpler analytical solutions and yet gave qualitatively similar results as those based on the no slip condition, thereby motivating the adoption of frictionless condition for parametric studies. The analytical model developed in this work can benefit the design, optimization and refinement for membrane-based adhesion systems such as adhesion measurement, transfer printing and soft robotic gripping.

Acknowledgements

X.Y. and R.L. acknowledge funding support from the National Science Foundation under the DMREF program (award number: 2118878). R.L. is also supported by a CAREER award from the National Science Foundation (award number: 1752449).

References

Begley, M.R., Collino, R.R., Israelachvili, J.N., McMeeking, R.M., 2013. Peeling of a tape with large deformations and frictional sliding. J. Mech. Phys. Solids 61, 1265–1279.

https://doi.org/10.1016/j.jmps.2012.09.014

Carlson, A., Wang, S., Elvikis, P., Ferreira, P.M., Huang, Y., Rogers, J.A., 2012. Active, programmable elastomeric surfaces with tunable adhesion for deterministic assembly by transfer printing. Adv. Funct. Mater. 22, 4476–4484. https://doi.org/10.1002/adfm.201201023

Chaudhury, M.K., Whitesides, G.M., 1991. Direct measurement of interfacial interactions between semispherical lenses and flat sheets of poly(dimethylsiloxane) and their chemical derivatives. Langmuir 7, 1013–1025. https://doi.org/10.1021/la00053a033

Cheng, Q.H., Chen, B., Gao, H.J., Zhang, Y.W., 2012. Sliding-induced non-uniform pretension governs robust and reversible adhesion: A revisit of adhesion mechanisms of geckos. J. R. Soc. Interface 9, 283–291. https://doi.org/10.1098/rsif.2011.0254

Collino, R.R., Philips, N.R., Rossol, M.N., McMeeking, R.M., Begley, M.R., 2014. Detachment of compliant films adhered to stiff substrates via van der Waals interactions: Role of frictional sliding during peeling. J. R. Soc. Interface 11, 20140453. https://doi.org/10.1098/rsif.2014.0453

Dening, K., Heepe, L., Afferrante, L., Carbone, G., Gorb, S.N., 2014. Adhesion control by inflation: Implications from biology to artificial attachment device. Appl. Phys. A Mater. Sci. Process. 116, 567–573. https://doi.org/10.1007/s00339-014-8504-2

Feng, W.W., Yang, W.H., 1973. On the contact problem of an inflated spherical nonlinear membrane. J. Appl. Mech. Trans. ASME 40, 209–214. https://doi.org/10.1115/1.3422928

Flory, A.L., Brass, D.A., Shull, K.R., 2007. Deformation and adhesive contact of elastomeric membranes. J. Polym. Sci. Part B Polym. Phys. 45, 3361–3374. https://doi.org/10.1002/polb.21322

Foster, H.O., 1967a. Very large deformations of axially symmetrical membranes made of neo-hookean materials. Int. J. Eng. Sci. 5, 95–117. https://doi.org/10.1016/0020-7225(67)90056-0

Foster, H.O., 1967b. Inflation of a plane circular membrane. J. Manuf. Sci. Eng. Trans. ASME 89, 403–407. https://doi.org/10.1115/1.3610067

Frey, S.T., Haque, A.B.M.T., Tutika, R., Krotz, E. V., Lee, C., Haverkamp, C.B., Markvicka, E.J., Bartlett, M.D., 2022. Octopus-inspired adhesive skins for intelligent and rapidly switchable underwater adhesion. Sci. Adv. 8, 1905. https://doi.org/10.1126/sciadv.abq1905

Gent, A.N., Kaang, S., 1986. Pull-off forces for adhesive tapes. J. Appl. Polym. Sci. 32, 4689–4700. https://doi.org/10.1002/app.1986.070320433

Guvendiren, M., Brass, D., Messersmith, P.B., Shull, K.R., 2009. Adhesion of DOPA-functionalized model membranes to hard and soft surfaces. J. Adhes. 85, 631–645. https://doi.org/10.1080/00218460902997000

Hart-Smith, L.J., Crisp, J.D.C., 1967. Large elastic deformations of thin rubber membranes. Int. J. Eng. Sci. 5, 1–24. https://doi.org/10.1016/0020-7225(67)90051-1

Hassager, O., Kristensen, S.B., Larsen, J.R., Neergaard, J., 1999. Inflation and instability of a polymeric membrane. J. Non Newton. Fluid Mech. 88, 185–204. https://doi.org/10.1016/S0377-0257(99)00018-X

Hiramoto, Y., 1963. Mechanical properties of sea urchin eggs: I. Surface force and elastic modulus of the cell membrane. Exp. Cell Res. 32, 59–75. https://doi.org/10.1016/0014-4827(63)90069-7

Hui, C.Y., Ruina, A., Long, R., Jagota, A., 2011. Cohesive zone models and fracture. J. Adhes. 87, 1–52. https://doi.org/10.1080/00218464.2011.538315

Hutchinson, J.W., Suo, Z., 1991. Mixed-mode cracking in layered materials. Adv. Appl. Mech. 29, 63–191. https://doi.org/10.1016/S0065-2156(08)70164-9

Johnson, K.L., Greenwood, J.A., 2013. Adhesive contact of elastic bodies: The JKR theory, in: Encyclopedia of Tribology. Springer, Boston, MA, pp. 42–49. https://doi.org/10.1007/978-0-387-92897-5_1086

Johnson, K.L., Kendall, K., Roberts, A.D., 1971. Surface energy and the contact of elastic solids. Proc. R. Soc. Lond. A 324, 301–313. https://doi.org/10.1098/rspa.1971.0141

Kendall, K., 1975. Thin-film peeling-the elastic term. J. Phys. D. Appl. Phys. 8, 1449–1452. https://doi.org/10.1088/0022-3727/8/13/005

Kendall, K., 1971. The adhesion and surface energy of elastic solids. J. Phys. D. Appl. Phys. 4, 1186–1195. https://doi.org/10.1088/0022-3727/4/8/320

Komaragiri, U., Begley, M.R., Simmonds, J.G., 2005. The mechanical response of freestanding circular elastic films under point and pressure loads. J. Appl. Mech. Trans. ASME 72, 203–212. https://doi.org/10.1115/1.1827246

Laprade, E.J., Long, R., Pham, J.T., Lawrence, J., Emrick, T., Crosby, A.J., Hui, C.Y., Shull, K.R., 2013. Large deformation and adhesive contact studies of axisymmetric membranes. Langmuir 29, 1407–1419. https://doi.org/10.1021/la303810d

Libai, A., Simmonds, J.G., 1998. The Nonlinear Theory of Elastic Shells. Cambridge University Press. https://doi.org/10.1017/cbo9780511574511

Long, R., Hui, C.Y., 2012. Axisymmetric membrane in adhesive contact with rigid substrates: Analytical solutions under large deformation. Int. J. Solids Struct. 49, 672–683. https://doi.org/10.1016/j.ijsolstr.2011.11.008

Long, R., Shull, K.R., Hui, C.Y., 2010. Large deformation adhesive contact mechanics of circular membranes with a flat rigid substrate. J. Mech. Phys. Solids 58, 1225–1242. https://doi.org/10.1016/j.jmps.2010.06.007

Newby, B.M.Z., Chaudhury, M.K., 1998. Friction in adhesion. Langmuir 14, 4865–4872. https://doi.org/10.1021/la9802901

Newby, B.M.Z., Chaudhury, M.K., 1997. Effect of interfacial slippage on viscoelastic adhesion. Langmuir 13, 1805–1809. https://doi.org/10.1021/la960962c

Newby, B.M.Z., Chaudhury, M.K., Brown, H.R., 1995. Macroscopic evidence of the effect of interfacial slippage on adhesion. Science 269, 1407–1408. https://doi.org/10.1126/science.269.5229.1407

Patil, A., Dasgupta, A., Eriksson, A., 2015. Contact mechanics of a circular membrane inflated against a deformable substrate. Int. J. Solids Struct. 67–68, 250–262. https://doi.org/10.1016/j.ijsolstr.2015.04.025

Patil, A., Nordmark, A., Eriksson, A., 2014. Free and constrained inflation of a pre-stretched

cylindrical membrane. Proc. R. Soc. A Math. Phys. Eng. Sci. 470, 20140282. https://doi.org/10.1098/rspa.2014.0282

Plaut, R.H., 2022a. Effect of pressure on pull-off of flat cylindrical punch adhered to circular membrane. J. Adhes. 98, 1438–1460. https://doi.org/10.1080/00218464.2021.1904911

Plaut, R.H., 2022b. Effect of pressure on pull-off of flat 1-D rectangular punch adhered to membrane. J. Adhes. 98, 1480–1500. https://doi.org/10.1080/00218464.2021.1908140

Plaut, R.H., White, S.A., Dillard, D.A., 2003. Effect of work of adhesion on contact of a pressurized blister with a flat surface. Int. J. Adhes. Adhes. 23, 207–214. https://doi.org/10.1016/S0143-7496(03)00013-7

Rivlin, R.S., Saunders, D.W., 1951. Large elastic deformations of isotropic materials VII. Experiments on the deformation of rubber. Philos. Trans. R. Soc. London. Ser. A, Math. Phys. Sci. 243, 251–288. https://doi.org/10.1098/rsta.1951.0004

Shanahan, M.E.R., 1997. A novel test for the appraisal of solid/solid interfacial interactions. J. Adhes. 63, 15–29. https://doi.org/10.1080/00218469708015211

Shull, K.R., 2002. Contact mechanics and the adhesion of soft solids. Mater. Sci. Eng. R Reports. https://doi.org/10.1016/S0927-796X(01)00039-0

Sohail, T., Tang, T., Nadler, B., 2013. Adhesive contact of a fluid-filled membrane driven by electrostatic forces. Int. J. Solids Struct. 50, 2678–2690. https://doi.org/10.1016/j.ijsolstr.2013.04.015

Song, S., Drotlef, D.M., Paik, J., Majidi, C., Sitti, M., 2019. Mechanics of a pressure-controlled adhesive membrane for soft robotic gripping on curved surfaces. Extrem. Mech. Lett. 30, 100485. https://doi.org/10.1016/j.eml.2019.100485

Song, S., Drotlef, D.M., Son, D., Koivikko, A., Sitti, M., 2021. Adaptive self-sealing suction-based soft robotic gripper. Adv. Sci. 8, 2100641. https://doi.org/10.1002/advs.202100641

Song, S., Drotlef, Di.M., Majidi, C., Sitti, M., 2017. Controllable load sharing for soft adhesive interfaces on three-dimensional surfaces. Proc. Natl. Acad. Sci. U. S. A. 114, E4344–E4353. https://doi.org/10.1073/pnas.1620344114

Song, S., Sitti, M., 2014. Soft grippers using micro-fibrillar adhesives for transfer printing. Adv. Mater. 26, 4901–4906. https://doi.org/10.1002/adma.201400630

Srivastava, A., Hui, C.Y., 2013. Large deformation contact mechanics of a pressurized long rectangular membrane. II. Adhesive contact. Proc. R. Soc. A Math. Phys. Eng. Sci. 469, 20130425. https://doi.org/10.1098/rspa.2013.0425

Swift, M.D., Haverkamp, C.B., Stabile, C.J., Hwang, D., Plaut, R.H., Turner, K.T., Dillard, D.A., Bartlett, M.D., 2020. Active membranes on rigidity tunable foundations for programmable, rapidly switchable adhesion. Adv. Mater. Technol. 5, 2000676. https://doi.org/10.1002/admt.202000676

Treloar, L.R.G., 1944. Stress-strain data for vulcanised rubber under various types of deformation. Trans. Faraday Soc. 40, 59–70. https://doi.org/10.1039/tf9444000059

Vajpayee, S., Hui, C.Y., Jagota, A., 2008. Model-independent extraction of adhesion energy from indentation experiments. Langmuir 24, 9401–9409. https://doi.org/10.1021/la800817x

Wan, K.T., 1999. Fracture mechanics of a v-peel adhesion test - Transition from a bending plate to a stretching membrane. J. Adhes. 70, 197–207. https://doi.org/10.1080/00218469908009555

Wan, K.T., Liu, K.K., 2001. Contact mechanics of a thin-walled capsule adhered onto a rigid planar substrate. Med. Biol. Eng. Comput. 39, 605–608. https://doi.org/10.1007/BF02345154

Wang, S.J., Li, X., 2007. The effects of tensile residual stress and sliding boundary on measuring the adhesion work of membrane by pull-off test. Thin Solid Films 515, 7227–7231. https://doi.org/10.1016/j.tsf.2007.02.098

Williams, J.G., 1997. Energy release rates for the peeling of flexible membranes and the analysis of blister tests. Int. J. Fract. 87, 265–288. https://doi.org/10.1023/A:1007314720152

Xu, D., Liechti, K.M., 2011. Analytical and experimental study of a circular membrane in adhesive contact with a rigid substrate. Int. J. Solids Struct. 48, 2965–2976. https://doi.org/10.1016/j.ijsolstr.2011.06.014

Yang, X., Yu, L., Long, R., 2021. Contact mechanics of inflated circular membrane under large deformation: Analytical solutions. Int. J. Solids Struct. 233, 111222. https://doi.org/10.1016/j.ijsolstr.2021.111222

Yu, H.H., He, M.Y., Hutchinson, J.W., 2001. Edge effects in thin film delamination. Acta Mater. 49, 93–107. https://doi.org/10.1016/S1359-6454(00)00293-7

Zhu, T., Li, G., Müftü, S., Wan, K.T., 2017. Revisiting the constrained blister test to measure thin film adhesion. J. Appl. Mech. Trans. ASME 84, 071005. https://doi.org/10.1115/1.4036776

Zhu, T., Müftü, S., Wan, K.T., 2018. One-dimensional constrained blister test to measure thin film adhesion. J. Appl. Mech. Trans. ASME 85, 054501. https://doi.org/10.1115/1.4039171